The Astrophysical Journal Supplement Series, 160:450–468, 2005 October

ROTATIONAL MODULATION OF X-RAY EMISSION IN ORION NEBULA YOUNG STARS

E. Flaccomio,[1] G. Micela,[1] S. Sciortino,[1] E. D. Feigelson,[2] W. Herbst,[3] F. Favata,[4]
F. R. Harnden, Jr.,[5,6] and S. D. Vrtilek[5]
Received 2005 February 1; accepted 2005 May 3

ABSTRACT

We investigate the spatial distribution of X-ray–emitting plasma in a sample of young Orion Nebula Cluster stars by modulation of their X-ray light curves due to stellar rotation. The study, part of the *Chandra* Orion Ultradeep Project (COUP), is made possible by the exceptional length of the observation: 10 days of ACIS integration during a time span of 13 days, yielding a total of 1616 detected sources in the $17' \times 17'$ field of view. We here focus on a subsample of 233 X-ray–bright stars with known rotational periods. We search for X-ray modulation using the Lomb Normalized Periodogram method. X-ray modulation related to the rotation period is detected in at least 23 stars with periods between 2 and 12 days and relative amplitudes ranging from 20% to 70%. In 16 cases, the X-ray modulation period is similar to the stellar rotation period, while in 7 cases it is about half that value, possibly due to the presence of X-ray–emitting structures at opposite stellar longitudes. These results constitute the largest sample of low-mass stars in which X-ray rotational modulation has been observed. The detection of rotational modulation indicates that the X-ray–emitting regions are distributed inhomogeneneously in longitude and do not extend to distances significantly larger than the stellar radius. Modulation is observed in stars with saturated activity levels ($L_X/L_{bol} \sim 10^{-3}$) showing that saturation is not due to the filling of the stellar surface with X-ray–emitting regions.

Subject headings: open clusters and associations: individual (Orion Nebula Cluster) — stars: activity — stars: low-mass, brown dwarfs — stars: pre–main-sequence — X-rays: stars

Online material: color figures, extended figure set, machine-readable table

1. INTRODUCTION

Pre–main-sequence (PMS) stars have high levels of X-ray activity with nonflaring X-ray luminosities up to 10^{31} ergs s^{-1} (Preibisch et al. 2005). As in the case of older cluster and field stars, X-ray activity in the PMS phase has often been attributed to a "scaled up" solar-like corona formed by active regions but more densely packed on the stellar surface and/or having higher plasma densities than on the Sun. For most nonaccreting PMS stars (weak-line T Tauri stars, or WTTSs), the fraction of energy emitted in the X-ray band with respect to the total stellar output, L_X/L_{bol}, is close to the saturation level, 10^{-3}, seen on rapidly rotating main sequence (MS) stars (Flaccomio et al. 2003a; Preibisch et al. 2005; Pizzolato et al. 2003). This suggests a common physical mechanism for the emission of X-rays or, at least, for its saturation in PMS and MS stars.

However, the solar analogy, while providing a simple picture of activity in PMS stars, may not be fully valid. Saturated PMS stars have $L_X/L_{bol} \sim 1000$ times greater than the Sun at its maximum, when the solar surface is ~50% covered with active regions and ~1% covered with active regions cores (Drake et al. 2000; Orlando et al. 2001). Plasma temperatures in saturated stars are much higher than on the Sun and, in the few cases where surface distributions can be determined, their active regions are concentrated at higher latitudes (e.g., Favata & Schmitt 1999; Jardine et al. 2002). The nature of the saturation phenomenon is not understood. It might be due to filling of the stellar surface with active regions, saturation of the magnetic reconnection process that heats the plasma, centrifugal limits on the coronal extent, concentration of magnetic fields toward the poles, or saturation of the internal dynamo generating the magnetic field that confines the plasma (Güdel 2004).

Even more puzzling than WTTSs are PMS stars that are still undergoing mass accretion (classical T Tauri stars, or CTTSs). CTTSs, with their circumstellar disks and magnetically funneled matter inflows and outflows host in general several different physical phenomena. With respect to X-ray activity, the bulk of the observational evidence points toward phenomena similar to those occurring on WTTSs. However, CTTSs have significantly lower and unsaturated values of L_X and L_X/L_{bol} (Damiani & Micela 1995; Flaccomio et al. 2003a, 2003b; Preibisch et al. 2005). Similar to saturated WTTSs, their X-ray activity does not correlate with stellar rotation, as seen in unsaturated MS stars and naturally interpreted in terms of a rotationally regulated α-Ω dynamo. A further complication is that the high-resolution X-ray spectra of two observed CTTSs, TW Hya (Kastner et al. 2002; Stelzer & Schmitt 2004) and BP Tau (Schmitt et al. 2005), indicate that a fraction of the soft X-ray luminosity may be produced in accretion shocks rather than coronal magnetic reconnection events.

In contrast to emission close to the stellar surface, some of the strongest flares seen in PMS stars are most easily explained by magnetic loops connecting the stellar surface with a circumstellar disk (Favata et al. 2005). Such loops arise naturally in models of magnetically driven accretion that seem to best explain the shapes of optical emission lines (Shu et al. 1994; Muzerolle et al. 2001). Magnetic reconnection in these loops might be the source of powerful and long-lasting X-ray flares

[1] INAF-Osservatorio Astronomico di Palermo Giuseppe S. Vaiana, Piazza del Parlamento 1, 90134 Palermo, Italy; ettoref@astropa.unipa.it.
[2] Department of Astronomy and Astrophysics, 525 Davey Laboratory, Pennsylvania State University, University Park, PA 16802.
[3] Department of Astronomy, Wesleyan University, Middletown, CT 06459.
[4] Astrophysics Division, Research and Science Support Department of ESA, Postbus 299, 2200 AG Noordwijk, Netherlands.
[5] Smithsonian Astrophysical Observatory, 60 Garden Street, Cambridge, MA 02138.
[6] Universe Division, Science Mission Directorate, NASA Headquarters.

(e.g., Shu et al. 1997; Montmerle et al. 2000). The influence of circumstellar disks and/or accretion on the emission of X-rays is not altogether unexpected given that the stellar magnetic field responsible for the confinement of X-ray–emitting plasma is likely affected by the circumstellar environment.

Observations of rotationally induced modulation of X-ray emission from low-mass stars can potentially yield valuable information on the extent and spatial distribution of the magnetic structures in active stars. Such observations are to date very scarce. X-ray rotational modulations have been seen in VXR 45, a fast rotating ($P_{\rm rot} = 0.22$ day) G9 ZAMS star (Marino et al. 2003), AB Dor (Hussain et al. 2005), a K0 ZAMS star with $P_{\rm rot} = 0.5$ day, and possibly EK Dra ($P_{\rm rot} = 2.7$ days) (Guedel et al. 1995). To the authors' knowledge, X-ray rotational modulation has not been to date reported for any PMS star. Because of the typical duration of X-ray observations, $\sim$1 day, it is indeed difficult to detect rotational modulation in the majority of stars, which have much longer periods.

The *Chandra* Orion Ultradeep Project (COUP)[7] has detected over 1616 sources in an 850 ks exposure spanning 13.2 days of the rich young Orion Nebula Cluster (ONC; Getman et al. 2005), well in the range of optically determined periods of PMS stars (Herbst et al. 2002). With COUP, we thus have the unique opportunity to study rotational modulation of X-ray emission on a large sample of PMS stars. We focus here on COUP sources whose rotation period is known from optical studies. Results from the analysis method discussed below are also presented for specific COUP sources by Stelzer et al. (2005) and Grosso et al. (2005).

The paper starts with a definition of the catalog of COUP sources with known rotation periods (§ 2). Section 3 describes the X-ray light curves and the analysis method used to estimate X-ray modulation periods and their reliability. Results of the period search are presented in § 4, followed by discussion of implications for the physical origin of X-ray activity in PMS stars (§ 5). Finally, in § 6 we summarize our results.

2. CATALOGS OF OPTICAL PERIODS

Our primary goal is to establish whether rotational modulation of X-ray emission is observed in COUP sources. Our initial sample comprises 295 COUP sources for which we could find in the literature a rotational period ($P_{\rm opt}$) determined from the periodic modulation of optical or near-infrared light curves.

We started with the list of 201 optical periods measured by Herbst et al. (2002) and reported by Getman et al. (2005) for COUP sources. Two of these COUP sources, 150 and 1328, are identified with close pairs: COUP 150 with sources 010-411 and 011-410 in Lucas & Roche (2000) and with sources 201 and 10342 in Herbst et al. (2002),[8] of which only 201 has a rotation period. COUP 1328 is associated with both 776a (with measured rotation period) and 776b in Hillenbrand (1997). In both cases, following Getman et al. (2005), we associated the X-ray source with the rotation period measured by Herbst et al. (2002) for one of the components. Our search for modulation in the X-ray light curves yields periods that appear related to these optically determined periods, thus confirming the association. We exclude the rotation period listed by Getman et al. (2005) for COUP 460, associated with source 347 in the catalog of Jones & Walker (1988) (JW), for which we could not find an optical period in the literature. Furthermore, we have updated the optical periods for COUP 1432 (JW 843, $P = 5.38$ days), 1443 (JW 852, $P = 1.32$ days) and 1487 (JW 883, $P = 5.70$ days), based on unpublished improved determinations by W. Herbst.

We then added periods from recent literature: 51 from Herbst et al. (2000); 15 from Stassun et al. (1999); 23 from the list of Carpenter et al. (2001) (selecting only periods with FAP $<$ 1%); 3 from Herbst et al. (2002) missed by Getman et al. (2005) (COUP 3 = JW 25, $P = 2.28$ days; COUP 68 = JW 130, $P = 1.2$ days; COUP 252 = JW 275a, $P = 0.95$ days); and 3 unpublished by W. Herbst (COUP 328 = JW 330, $P = 4.08$ days; COUP 1350 = JW 795, $P = 2.80$ days; COUP 1154 = JW 684, $P = 3.35$ days).

Table 1 lists the 295 COUP sources that are thus assigned a rotational period. In cases when more than one optical period was retrieved from the literature, we list other values if differing by more than 10% from the adopted one.

3. X-RAY LIGHT CURVES AND ANALYSIS METHOD

Adopting the source photon extraction of the ACIS X-ray data presented in Getman et al. (2005), we bin arrival times and compute the count rate in each bin taking into account gaps in the observation. We then subtract the mean background count rate[9] as determined from a source-free region close to each source (Getman et al. 2005). The period analysis described below was originally performed with bin lengths of 10,000, 5000, and 2000 s. Results obtained in the three cases were very similar, both regarding the modulation periods found and their statistical significances, though slightly better significances were obtained with shorter bin lengths, probably as a result of an improved ability to account for nonrotationally induced variability (e.g., flares). In the following, we therefore refer exclusively to the analysis performed using 2000 s bins.

Our goal is to detect rotational modulation in the X-ray light curves of COUP sources. We have initially considered two period analysis methods: the Lomb Normalized Periodogram (LNP) method (Scargle 1982) and the string length method (SLM) with length defined as in Lafler & Kinman (1965), but we soon realized that the former gave better results. The LNP is the traditional Schuster (1898) periodogram of Fourier analysis adjusted for gaps in the data: a function is computed from the data for a range of test frequencies and the frequency that maximizes this function is considered as the most likely frequency in the data.

In order to estimate the range of applicability of the LNP analysis to our data, we first performed a series of simple simulations by generating purely periodic light curves in 2000 s bins with the observed window function. Three light curve shapes were considered: a sinusoid ($M[1 + A \sin \omega t]$), a three-level ($M[1 - A]$, M, $M[1 + A]$) step function, and a two-level ($M[1 - A]$, $M[1 + A]$) step function. Simulated periods ranged from 0.5 to 30 days and relative amplitudes (A) from 10% to 90%. Noise was assumed Poissonian, appropriate for total source counts ranging from 100 to 10^5. One hundred replicates were run for each set of input parameters. Figure 1 shows the results for the cases of sinusoidal light curves and $A = 30\%$ and $A = 90\%$. The plots show the median and the 1 σ dispersion of the ratio between the period corresponding to the main LNP peak ($P_{\rm out}$) and the input

[7] Links to the COUP data set are available in the electronic edition of the *Supplement*.

[8] Entries for source 201 and 10342 in Herbst et al. (2002) are very similar, and they might actually refer to the same object, but only 201 has a rotation period. Sources 010-411 and 011-410 in Lucas & Roche (2000) are 1.″1 apart (seeing $\sim$0.″6) and have similar magnitudes and colors. The H magnitudes add up to the 2MASS value of 10.6, but the J magnitudes add up to 10.05, while 2MASS gives 11.48.

[9] For all sources the background rate is statistically indistinguishable from being constant within the observation.

TABLE 1
DATA

COUP Number (1)	NetCts[a] (2)	ID (3)	P_{opt} (days) (4)	Reference[b] (5)	Mass ($M_\odot$) (6)	log Age (yr) (7)	log L_X (ergs s^{-1}) (8)	log L_X/L_{bol} (9)	EW (Ca II) (10)	Mod. Flag[c] (11)
3.....	15	25	2.28	H	0.17	5.9	28.2	−4.5	0.0	†
6.....	1887	40	9.81	H	0.23	6.3	29.8	−3.2	0.0	LH
17.....	1083	63	4.10	cs	0.90	6.1	30.1	−3.8	1.9	
20.....	382	70	1.50	H	0.16	5.3	29.4	−3.7	0.0	†
23.....	55449	75	3.45	h	2.17	6.2	31.3	−3.2		
27.....	5948	77	1.50[d]	cshH	0.53	6.2	30.3	−3.1	1.8	†
28.....	20863	81	4.41	H	0.53	6.0	30.9	−2.6	1.6	L
29.....	2287	83	7.72	sh	0.33	6.1	30.0	−3.3	−9.2	
30.....	169	84	2.45	H	0.25	6.4	28.8	−4.1	0.0	
41.....	574	98	2.34	H	0.21	6.0	29.3	−3.7	0.0	

NOTES.—Col. (1): COUP source number; col. (2): net, background-subtracted, ACIS counts; col. (3): optical source identification (Hillenbrand 1997; Herbst et al. 2002); col. (4): rotation period; col. (5): reference for the rotation period; col. (6): stellar mass; col. (7): log stellar age; col. (8): log L_X; col. (9): log L_X/L_{bol}; col. (10): Ca II line equivalent width; col. (11): X-ray modulation flag. Table 1 is available in its entirety in the electronic edition of the *Astrophysical Journal Supplement*. A portion is shown here for guidance regarding its form and content.

[a] Net photons collected during the 850 ks COUP observation in the source extraction area, including from 1% to 96% of the source point spread function (∼90% for most sources; Getman et al. 2005).

[b] References for P_{opt}: (H) Herbst et al. 2002; (h) Herbst et al. 2000; (s) Stassun et al. 1999; (c) Carpenter et al. 2001; (U) Herbst, unpublished.

[c] Indicates filtered light curves (N, L, or H) for which the LNP analysis yielded FAP < 0.1%. A dagger (†) indicates that the periodogram analysis was not performed because either $P_{opt} < 2.0$ days or counts < 100.

[d] Other period: 2.99(c).

period P_{in} as a function of input period and simulated source counts. Note that, at this stage, we are not yet estimating significances for the peaks in the periodograms as in the more sophisticated simulations discussed in § 4.2. The simulations here indicate that a certain fraction of the P_{out} will be unrelated to P_{in} when the statistics and/or the amplitudes are too low. In the $A = 30\%$ case, for example, the curves referring to the 100 count light curves lie outside the plot vertical scale. For high count rates, the median P_{out}/P_{in} does not diverge by more than 0.03 dex for $P_{in} < 13$ days, the length of the observation (including gaps in the data stream). For simulations with 100 (1000) counts, the minimum amplitude that still yields $P_{in}/P_{out} \sim 1$ for $P_{in} < 13$ days is $A \sim 60\%$ (20%). Similar results are obtained if the shape of the simulated modulation is changed from a sinusoid to a 2 or 3 level step function.

Given these results, in the analysis of real data we therefore decided to limit our search to X-ray periods P_X shorter than 13 days. The lower limit to the accessible P_X is set by timescales

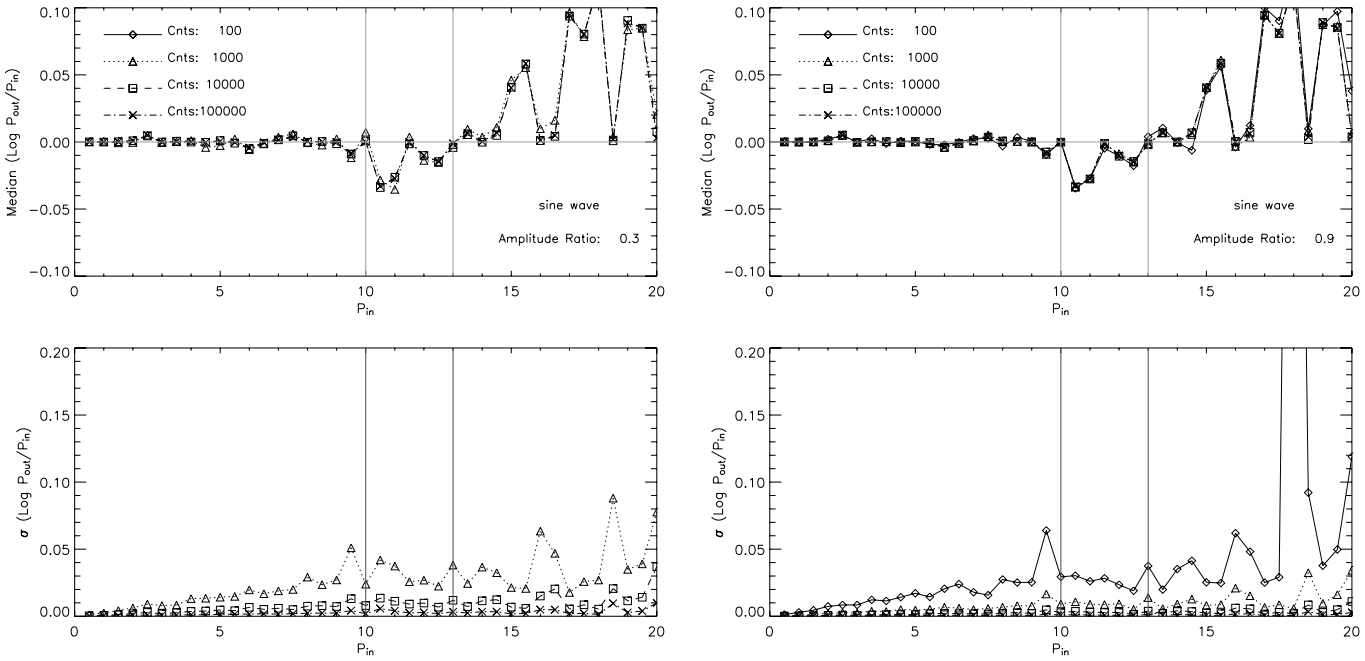

FIG. 1.—Results of simulations of purely periodic sinusoidal light curves for relative modulation amplitudes of 30% (*left*) and 90% (*right*). *Upper panels*: log median P_{in}/P_{out}, as a function of P_{in}; P_{in} is the input period for the simulation and P_{out} is the period corresponding to the main peak in the resulting periodogram. Each point is the result of 100 simulated sinusoidal light curves with counts ranging from 100 to 100,000, as indicated in the label. Vertical lines indicate periods of 10 and 13 days, i.e., the exposure time and the total length of our observation including gaps. *Lower panels*: 1 σ scatter of the 100 simulation around the median for the same simulations.

of the nonrotational variability present in our data, notably flares. Because of variability unrelated to rotation, the simulation discussed above represent a best case scenario and can only indicate a lower limit to the typical uncertainties in the determination of periods. In § 4.2, after presenting the results of the LNP analysis of COUP sources, we introduce more realistic simulations of light curves that include flares.

3.1. *Calculation of FAPs and Filtering of Light Curves*

The most difficult part of the periodogram analysis in the nonideal case is establishing the significance of the peaks found in the LNP or, more specifically, the false alarm probabilities (FAPs). Stochastic noise and intrinsic variability, unrelated to rotational modulation, can produce spurious features in the LNP that can easily be mistaken for real modulation. A simple example, which recurs frequently in our data, is that of repeated flares. Two bright flares occurring on the same source within our observation with a temporal separation ΔT will produce a spurious peak in the periodogram at frequency $1/\Delta T$. It is therefore paramount to either take into account the nonrotationally induced variability in the calculation of the FAPs and/or to filter out identifiable features from the light curves prior to the calculation of the LNP.

In the presence of uncorrelated noise, FAPs can be computed from the actual light curve through a permutation resampling technique. A large number of artificial light curves are computed by replacing actual count rates with values randomly chosen from the same light curve. The LNP analysis is then performed on each of these realizations and, for each frequency, the distribution of power values is recorded. Once the maximum from the real periodogram is found, its value can be compared to the distribution obtained, at the same frequency, from the randomized light curves in order to establish the probability that values as high as the observed one are due to random fluctuations; this is the FAP.

Performing this calculation for our X-ray light curves always results in vanishingly small FAPs, indicating that LNPs of COUP sources present peaks that cannot be explained by purely stochastic noise. This arises because flares with a variety of characteristics are ubiquitous (Wolk et al. 2005; Favata et al. 2005), as well as less well-understood temporal phenomena. We therefore seek to compute FAPs by randomizing any periodic component of the light curves but preserving these other correlated features. We define blocks of adjacent temporal bins with total length $\tau_{\rm corr}$ and randomize the position of these blocks. Our $\tau_{\rm corr}$ should be longer than flare timescales and shorter than rotational periods, but these two conditions cannot always be simultaneously achieved. We choose $\tau_{\rm corr} = 8$ hr and consequently limit our search of peaks in the periodograms to periods longer than 1 day. We caution that the choice of $\tau_{\rm corr} =$ 8 hr is somewhat arbitrary and a number of longer flares are observed (Favata et al. 2005). For this reason the FAPs that we derive are not formally accurate, but we are confident they are good indicators of the relative significance of the peaks in the periodograms.

An essential element of our analysis is to perform periodogram analysis on both the original light curves and those where large flares are removed. We filter the light curves using two trimming levels established to qualitatively remove obvious flares: (1) a light trimming ("L") of bins with count rates higher than 1.5 times the 13% upper quantile of the count rate distribution; and (2) a heavy trimming ("H") of bins with count rates higher than 1.5 times the 25% quantile. We also tried filtering out time interval that are identified as belonging to flares using maximum-likelihood blocks as described in Wolk et al. (2005), but, except for a few sources, results were not in general better than with the simpler count rate trimming procedures. The original light curves will be referred to as "N" (no filter). Given the large variety of behaviors observed in our light curves, we have not been able to identify a single best filtering method for all cases. Moreover, our filtering may not always improve our ability to find real modulation periods and to reject spurious results due, for instance, to the alignment of untrimmed flare decay tails.

Given the above considerations on the possible pitfalls involved in the search for true modulation periods in the complex X-ray light curves of COUP sources, we adopt the following graduated levels of confidence in a possible rotational period detection: periodogram peaks are considered most significant when FAP $< 0.1\%$[10] in all three (N, L, and H) light curves. Less confidence is given to sources in which FAP $< 0.1\%$ in any of the three light curves. When more than one filtering strategy exhibit a signal, we adopt the period with the lowest FAP.[11]

4. RESULTS

Table 1 lists optical and X-ray data for the 295 COUP sources with known optical rotation periods. The period values are described in § 2, and the remaining columns are obtained from tables in Getman et al. (2005). We performed the LNP period analysis for 233 of these sources; 21 sources with $<$100 X-ray photons and 41 sources with optical rotation period $P < 2$ days were omitted from analysis. This is to exclude stars for which period detection would likely be hampered by low photon statistics and by the similarity between the flare and modulation timescales. For the 233 analyzed sources, the last column indicates whether a FAP $< 0.1\%$ peak is seen in the periodogram of the N, L, and H light curves. One hundred and nine sources are detected as periodic in at least one data set (we call this the "N+L+H" sample), 48 sources of these are detected as periodic using unfiltered (the N sample) light curves, and 34 of these are the highest confidence periodic signals showing a significant peak in all three data sets (the "N·L·H" sample). Detailed results of the periodogram analysis for the N·L·H sample are given in Table 2. For each source, we provide modulation periods and FAPs for each of the three X-ray light curves. The lowest FAP value (highest significance period) was obtained from the unfiltered light curves in 4 sources, lightly filtered light curves in 15 sources, and heavily filtered light curves in 15 sources (col. [12] of Table 2).

Column (13) in Table 2 reports an estimate for the relative amplitude of the modulation from the folded X-ray light curve derived from the light curve giving the lowest FAP. In order to reduce random fluctuations when estimating amplitudes, we rebin the phased light curve to give 8 bins per modulation cycle if the light curve has less than 8000 counts and an average of 1000 counts per bin for brighter sources. The relative amplitude is then defined as the difference between the minimum and maximum count rates divided by the sum of the same quantities. Resulting values are uniformly distributed between $\sim$20% and $\sim$70%.

Figures 2, 3, and 4 show results in four panels for six illustrative COUP sources, three of which belong to the N·L·H sample. We show: the original unfiltered light curves, the LNP

[10] FAPs were computed with the bootstrapping procedure described in this section using 100,000 iterations, sufficient to define the 0.1% level.

[11] In 7 cases more than one LNP peak has FAP $= 0.0\%$ within the precision of the determination. In these cases we choose the highest LNP peak above the FAP $= 0.1\%$ threshold.

TABLE 2
RESULTS OF THE PERIOD ANALYSIS: N·L·H SAMPLE

COUP Number (1)	NetCts[a] (2)	ID (3)	P_{opt} (4)	Reference[b] (5)	P_X^N (6)	FAP (7)	P_X^L (8)	FAP^L (9)	P_X^H (10)	FAP^H (11)	B (12)	Amp. (13)	Class (14)
62	9294	123	6.63	s	8.13	0.06	9.09	0.00	11.51	0.03	L	0.72	1
131	9038	187	14.41	H	7.92	0.01	7.70	0.01	1.97	0.01	N	0.71	$\frac{1}{2}$
139	6094	192	9.04	sH	4.87	0.00	4.91	0.00	4.91	0.00	N	0.50	$\frac{1}{2}$
161	2428	211	5.46	sH	5.71	0.02	5.92	0.04	5.79	0.01	H	0.18	1
174	2810	222	5.17	shH	4.72	0.03	4.66	0.00	4.68	0.00	H	0.33	1
226	2676	258	10.98	cH	12.10	0.01	11.91	0.01	10.66	0.05	N	0.58	1
250	497	278	6.76	H	6.39	0.00	6.82	0.00	6.71	0.00	H	0.53	1
271	189	292	5.11	c	2.68	0.04	2.33	0.01	2.33	0.00	H	0.66	$\neq$
292	1580	...	7.83	c	10.39	0.00	10.00	0.00	9.83	0.00	L	0.61	1
413	3204	362	2.73	hH	6.79	0.06	6.72	0.01	6.09	0.02	L	0.47	$\neq$
454	17125	373	9.81	H	3.91	0.01	3.92	0.01	3.99	0.05	N	0.53	$\neq$
612	2305	435a	10.33	c	2.98	0.02	3.02	0.01	3.03	0.00	H	0.20	$\neq$
697	5984	470	10.70	h	9.62	0.00	9.93	0.00	10.22	0.00	H	0.38	1
1023	4852	9250	2.27	H	12.18	0.03	11.92	0.03	11.63	0.02	H	0.26	$\neq$
1070	4733	634	5.38	H	3.53	0.05	3.61	0.01	3.61	0.00	H	0.28	$\neq$
1116	52865	660	6.15	h	6.64	0.02	6.64	0.02	6.64	0.02	H	0.26	1
1141	874	9280	7.92	H	4.12	0.02	4.18	0.01	4.20	0.01	L	0.45	$\frac{1}{2}$
1161	9270	690	3.90	H	3.43	0.02	9.53	0.00	9.83	0.00	L	0.46	$\neq$
1216	637	721	2.45	h	6.55	0.05	6.76	0.04	6.63	0.08	L	0.49	$\neq$
1233	1056	727	6.03	h	8.40	0.01	8.20	0.00	8.20	0.04	L	0.58	1
1248	14567	733	3.28	sH	6.16	0.03	6.15	0.03	6.15	0.06	L	0.36	$\neq$
1335	5466	782	10.22	c	5.69	0.03	5.55	0.02	5.56	0.00	H	0.33	$\frac{1}{2}$
1355	5878	798	10.36	H	11.96	0.01	12.14	0.01	5.19	0.07	L	0.47	1
1382	10217	811a	11.10	h	5.61	0.00	5.61	0.00	5.63	0.00	H	0.25	$\frac{1}{2}$
1384	25433	813	2.85	cshH	2.79	0.08	2.87	0.06	2.87	0.06	H	0.44	1
1398	3037	823	9.00	hH	10.79	0.01	10.31	0.00	9.94	0.00	L	0.61	1
1421	6370	836	12.20	h	4.38	0.05	4.39	0.02	4.39	0.04	L	0.26	$\neq$
1423	3553	838	7.75	H	6.88	0.06	6.87	0.01	6.85	0.00	H	0.29	$\neq$
1429	5527	839	7.52	hH	8.22	0.01	8.09	0.00	8.04	0.00	L	0.30	1
1448	3304	860	6.33	cshH	7.82	0.06	7.89	0.00	7.97	0.00	H	0.30	1
1463	8214	867	10.66	H	11.20	0.09	3.95	0.10	10.87	0.07	H	0.34	1
1500	4438	892	8.56	hH	10.40	0.00	10.43	0.00	10.90	0.00	L	0.50	1
1570	4146	962	9.56	cH	4.99	0.00	4.97	0.00	4.92	0.01	L	0.63	$\frac{1}{2}$
1590	1190	982	7.10	c	3.59	0.02	3.62	0.01	3.49	0.01	L	0.50	$\frac{1}{2}$

NOTES.—Col. (1): COUP source number; col. (2): net, background-subtracted, ACIS counts; col. (3): optical source identification (Hillenbrand 1997; Herbst et al. 2002); col. (4): rotation period; col. (5): reference for the rotation period; cols. (6), (8), (10): best X-ray period from the N, L, and H analyses; cols. (7), (9), (11): FAPs for the best X-ray periods in N, L, and H analyses; col. (12): analysis that yielded the lowest FAP; col. (13): relative amplitude of the modulation computed from the averaged folded light curve as (max−min)/(max+min); col. (14): source class according to P_X/P_{opt}.

[a] Net photons collected during the 850 ks COUP observation in the source extraction area, including from 1% to 96% of the source point spread function (∼90% for most sources; Getman et al. 2005).

[b] References for P_{opt}: (H) Herbst et al. 2002; (h) Herbst et al. 2000; (s) Stassun et al. 1999; (c) Carpenter et al. 2001.

periodograms for the best filtering strategy (i.e., lowest FAP), and light curves folded with both the best X-ray period and the previously known optical period. Similar figures for the 34 N·L·H sources in Table 2 are presented in Figure Set 5.

4.1. *Statistical Comparison of P_{opt} versus P_X*

The three panels in Figure 6 compare the optical and X-ray periods for the three different subsamples discussed in the previous section: the 109 N+L+H sources showing FAP $< 0.1\%$ in at least one filtered data set; the 48 N sources showing periodicity in the unfiltered data set; and the 34 N·L·H sources. For the least reliable N+L+H sample, no clear relationship between the X-ray and optical periods is seen, but for the high confidence N·L·H sample, most of sources align close to the $P_X = P_{opt}$ and the $P_X = 0.5P_{opt}$ loci.

To better define this effect, the distribution of ratios between X-ray and optically determined periods is investigated in Figure 7. Vertical lines indicate ratios of 1/4, 1/2, 1, 2, and 4. In all samples, we see a main peak corresponding to roughly equal X-ray and optical periods and a smaller but narrower peak corresponding to $P_X \sim 0.5P_{opt}$. We interpret these plots as evidence that a substantial fraction of the X-ray periods are indeed related to the optically determined rotation periods, even though one is often an harmonic of the other. To strengthen this conclusion, we show in Figure 8 the distribution of P_X/P_{opt} for X-ray sources that did not pass our significance test, i.e., those for which FAP $> 0.1\%$ in all three "N," "L," and "H" analyses (*top*), 'N' (*center*), and any of "N," "L," or "H" (*bottom*). These distributions show little or no relation between optical and X-ray modulation, giving confidence that the FAP $> 0.1\%$ criterion is indeed effective in preferentially selecting true X-ray modulation periods.

To facilitate discussion, we distinguish three types of COUP sources: "class 1" when the X-ray and optical periods are nearly equal, $-0.05 < \log P_X/P_{opt} < 0.15$; "class $\frac{1}{2}$" when the X-ray period is half of the optical period, $-0.3 < \log P_X/P_{opt} < -0.25$; and "class $\neq$" for all other stars. The light curves and periodograms in Figures 2–4 show two examples of each

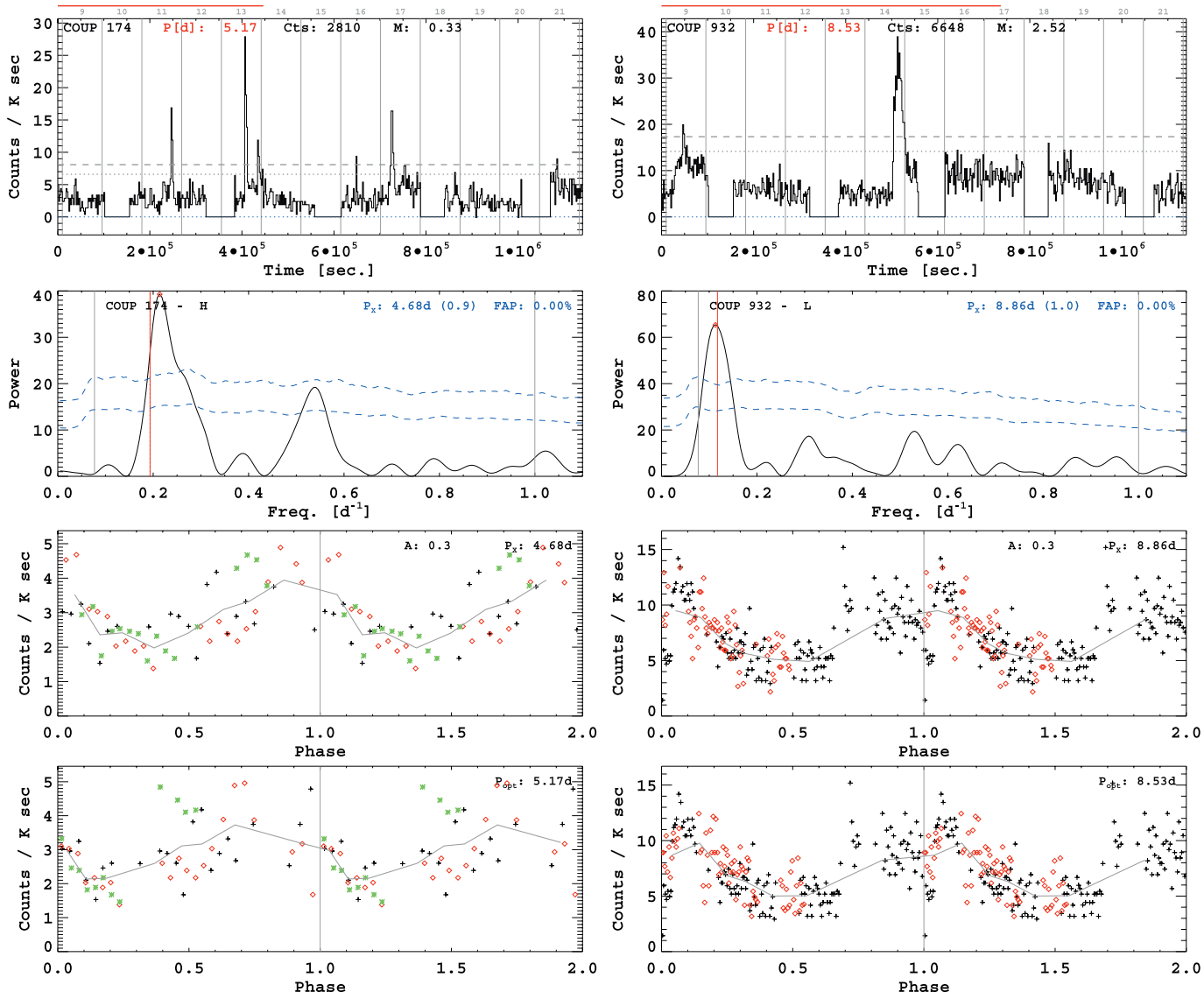

FIG. 2.—*Top panels*: Light curves for two sources (COUP 174 and COUP 932) for which the modulation analysis yielded X-ray periods similar to optically determined stellar rotation periods. Background-subtracted count rates in 2000 s bins are plotted vs. the time since the beginning of the observation. UT dates (in 2003 January) are given above the plot, between gray vertical lines indicating UT midnights. Source number, optical periods, extracted net counts, and stellar mass are given in the upper part of the plot. The red horizontal segment above light curves indicates the length of one rotation period. The dashed and dotted horizontal lines indicate count-rate thresholds used for "light trimming" and "heavy trimming," respectively. *Second row of panels*: Lomb Normalized Periodograms for the light curves filtered so as to minimize the FAP. The filtering method (N = none; L = light trimming; H = heavy trimming) is given next to the source ID in the upper right corner. The red vertical line indicates the frequency corresponding to the optical rotation period. The two dashed curves indicate 1% and 0.1% FAP thresholds (see text). The most likely X-ray period is reported in the upper right corner (with in parenthesis the ratio P_X/P_{opt}) along with the FAP. *Third row*: light curves folded with the most likely X-ray period, reported in the upper right corner along with the relative modulation amplitude. Different symbols and colors indicate data points belonging to different modulation cycles. The solid gray line indicate the average count rate as a function of phase. *Bottom panels*: light curves folded with the optically determined rotation period.

class. These classifications are listed in the last column of Table 2. Out of the 109 sources in sample N+L+H, 38, 14, and 57 belong to classes 1, $\frac{1}{2}$, and $\neq$, respectively. Out of the 34 sources in sample N·L·H, 16, 7, and 11 fall in the same classes.[12]

In addition to the expected finding of X-ray periods similar to the optical periods, we thus unexpectedly find X-ray periods half as long as established optical periods as well as a number of X-ray periods apparently unrelated to the stellar rotation. Moreover, within class 1 and $\frac{1}{2}$ sources, there is also a possible systematic shift such that P_X-values are longer than P_{opt} or $0.5P_{opt}$ (Fig. 6).[13] It remains to be seen, however, whether these unexpected features in the P_X/P_{opt} ratio histogram are spurious effects due to the characteristic of the data and/or the analysis method we have applied.

4.2. *Verification of the Method through Simulations*

Due to the complexity of the COUP light curves and of our analysis procedures, in order to better understand our results,

[12] In some LNP periodograms of class $\neq$ sources, secondary peaks corresponding to $\sim P_{opt}$ or to $\sim 0.5P_{opt}$ are present. If we were to consider these secondary peaks as true modulation periods, seven class $\neq$ sources in the N+L+H sample and one in the N·L·H sample would be upgraded to class 1.

[13] We estimate the significance of the shifts, computing the mean $\log P_X/P_{opt}$ and its uncertainty in symmetrical intervals centered on 0 and $\log 0.5$. The shifts are most significant in the N sample: 3.2 σ for the $P_X/P_{opt} \sim 1$ peak and 4.8 σ for the $P_X/P_{opt} \sim 0.5$ peak.

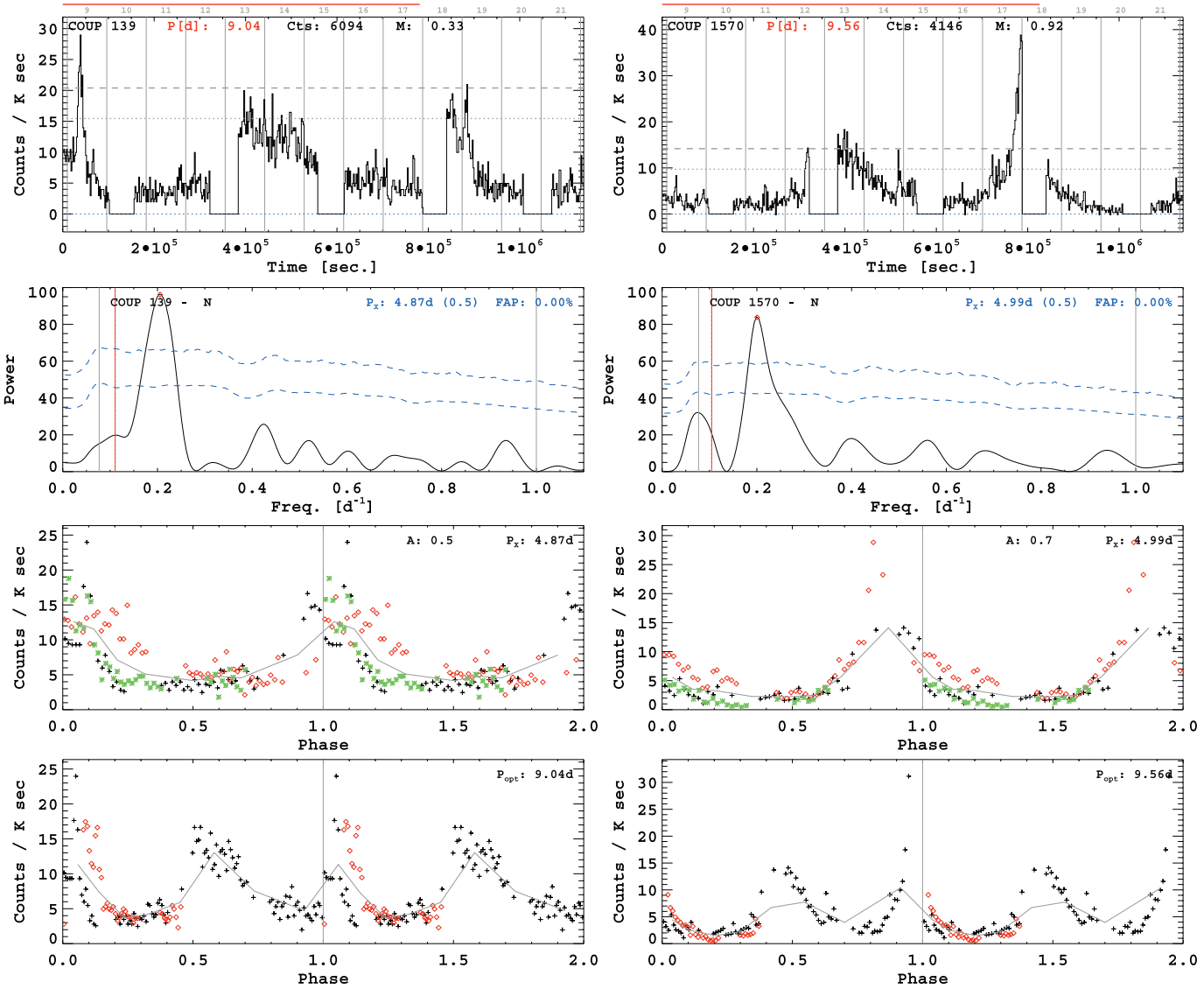

FIG. 3.—Same as Fig. 2, but for two sources for which the most likely X-ray period is half the optical period. Note, however, that for the source on the left (COUP 139) a not significant peak is present at the optical period. Applying the "H" filter, the peak at $P \sim 4.9$ days remains predominant but the FAP of this secondary peak drops to 0.7%.

we have performed extensive Monte Carlo simulations of modulated and unmodulated light curves that try to reproduce the essential characteristics of our data. Construction of these simulated light curves, which include the complications of gaps in the *Chandra* exposure and flares in the COUP stars, are described in the Appendix. We then applied our full analysis method described in § 3 to these simulated light curves. Here we summarize the main findings.

The dashed lines in Figures 7 and 8 indicate the expected outcome of our period analysis on simulated light curves that have no intrinsic periodicity, for reasonable choices of model input parameters. In each panel, different lines refer to different values of the parameters that determine the flare frequency distribution, the light curve statistics and the decay time of flares, all chosen so as to yield light curves that are reasonably similar to the observed ones (specifically, in particular, $\alpha = 2.50$, NF = [500, 1000], $\tau_{\rm fl} = [5, 8]$hr; see Appendix). In all cases, these $P_{\rm X}/P_{\rm opt}$ distributions do not show any sharp peak around 1.0 and 0.5 as we observe in the COUP data. We conclude that the presence of these peaks must be due to intrinsic source modulation. The fact that they occur at values of $P_{\rm X}/P_{\rm opt} \sim 1.0$ and 0.5, and not at any other values, is a further support that the X-ray modulations are real and related to stellar rotation.

In another important series of simulations we introduced periodic modulations into the simulated light curves. These simulations show that the observed spread in $\log P_{\rm X}/P_{\rm opt}$ among class 1 sources can be attributed to uncertainties in the analysis procedure. Moreover, all simulation series show that a fraction of sources show FAP $< 0.1\%$ periods randomly distributed between $0.2 < P_{\rm X}/P_{\rm opt} < 5$. This can explain the observed sources with widely distributed $P_{\rm X}$-values in Figures 6 and 7. Our simulations do not, however, reproduce the subtle effect that $P_{\rm X}$-values tend to be slightly longer than $P_{\rm opt}$ in class 1 sources. Even more importantly they also fail to reproduce the second peak around $P_{\rm X}/P_{\rm opt} = 0.5$.

The fact that our simulations retrieve some of the fundamental characteristics of the real data after our complicated data analysis procedures lends strong support to the basic result that the class 1 and $\frac{1}{2}$ COUP sources are truly periodic with periods intrinsically related to the optical rotational periods.

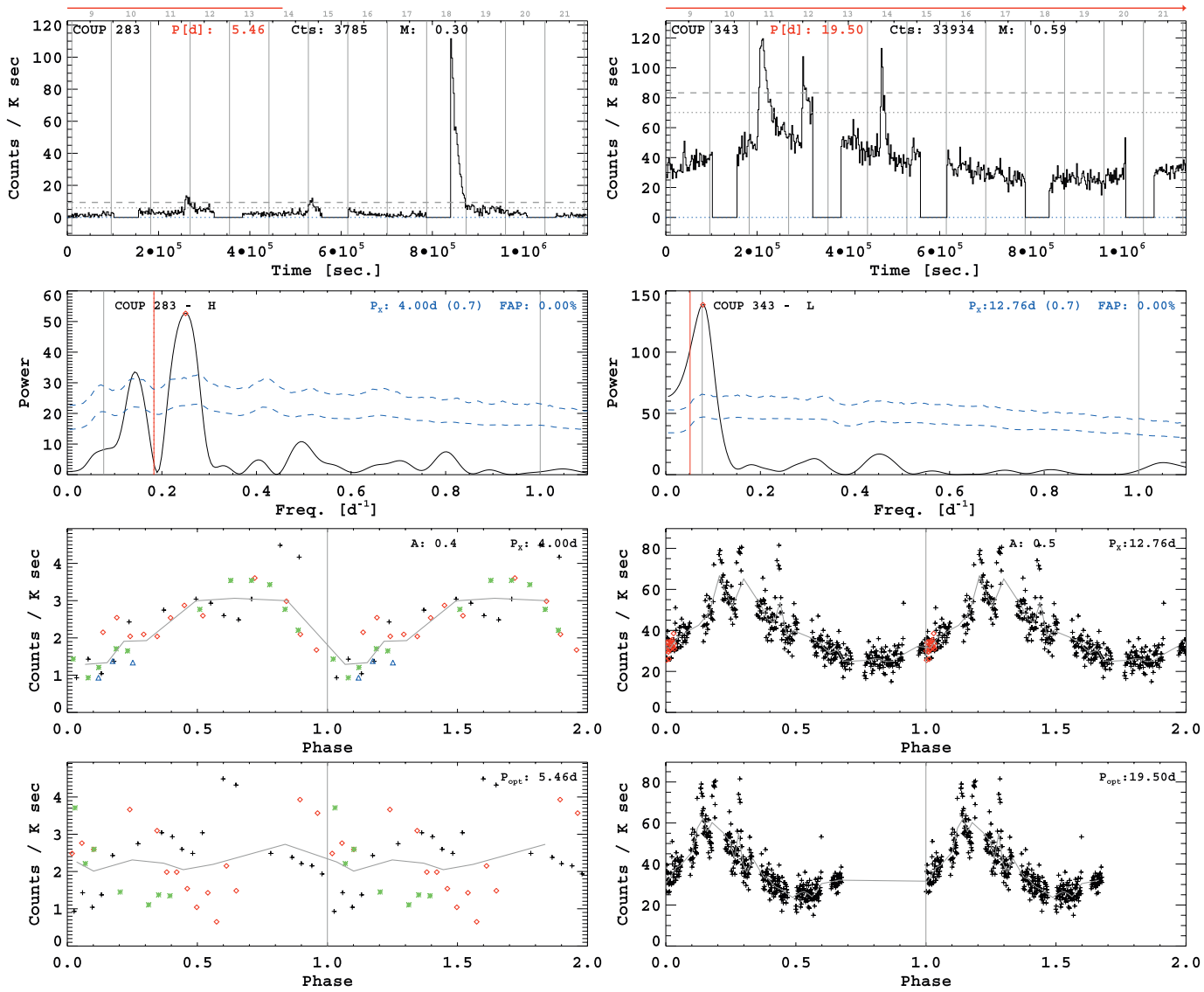

FIG. 4.—Same as Fig. 2, but for two sources for which the most likely X-ray periods is apparently unrelated to the optical one.

4.3. *Physical Properties of Modulated Stars*

We now return to the physical properties of the stars listed in Table 1 to investigate possible relationships to the stars showing rotational modulation. The "modulated" subsample showing rotational periodicities are the 23 class 1 and $\frac{1}{2}$ stars in the N·L·H sample.[14] We compare these to the full sample of COUP sources searched for periodicities; i.e., the 233 "searched" sources with known $P_{\rm rot}$, $P_{\rm rot} > 2$ days and with more than 100 detected counts. Moreover, in order to understand possible biases in this latter sample, we will compare the "searched" sample to the "global" sample of COUP sources with more than 100 COUP counts.

Figure 9 shows the Hertzsprung-Russell diagram for these three samples. A comparison of the mass and age distributions of the "searched" and "global" samples indicate that the former is preferentially deficient in very low-mass stars and also in the youngest population. This may be understood as a selection effect: very low-mass stars are both less likely to have detected optical modulations and have >100 COUP counts than more massive stars (Fig. 10*a*). Moreover, measurement of $P_{\rm rot}$ through optical modulation may be impeded at the earliest stellar evolutionary stages due to high stochastic variability related to mass accretion. Compared to the "searched" sample, stars in the "modulated" samples appear to occupy the same area in the HR diagram and to span the full range of stellar masses and ages. This is confirmed by two-sided Kolmogorov-Smirnov (KS) tests that do not allow rejection of the null hypothesis that the distributions of masses and ages are drawn from the same parent population.

Figures 10*a* and 10*b* show the run of $L_{\rm X}$ and $L_{\rm X}/L_{\rm bol}$ with stellar mass for the same samples. We observe that, respect to the "global" sample, stars in the "searched" sample, i.e., with optical rotation periods, have larger than average $L_{\rm X}$ and $L_{\rm X}/L_{\rm bol}$ and this is confirmed with high significance by a statistical comparison of the distributions of $\log L_{\rm X}$ and $\log (L_{\rm X}/L_{\rm bol})$. This bias was noticed before (Flaccomio et al. 2003b; Stassun et al. 2004) and might be due to a positive correlation between coronal activity and presence of stellar spots responsible for the modulation in the optical band. We note that the bias appears to be stronger in $L_{\rm X}/L_{\rm bol}$; this could result because, given a fixed photometric precision, the probability of detecting an optical modulation depends on the contrast between spot coverage (likely

[14] Note that we will not consider sources in class $\neq$. The simulations described in § 4.2 indicate that most are likely to be spurious period detections.

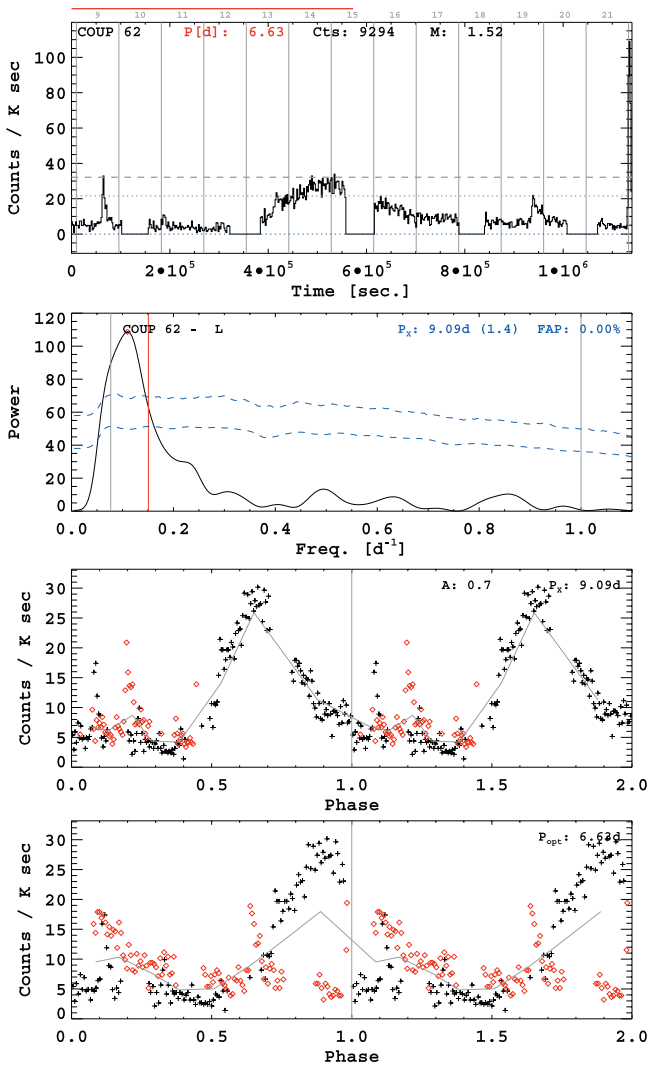

FIG. 5.1. COUP 62.

FIG. SET 5.—*Top panel*: Background-subtracted light curve; count rates in 2000 s bins are plotted vs. the time since the beginning of the observation. UT dates (in 2003 January) are given above the plot, between gray vertical lines indicating UT midnights. The source number, optical period, extracted net counts, and stellar mass are given in the upper part of the plot. The red horizontal segment above light curves indicates the length of one rotation period. The dashed and dotted horizontal lines indicate count-rate thresholds used for "light trimming" and "heavy trimming," respectively. *Second panel*: Lomb Normalized Periodogram for the light curves filtered so as to minimize the FAP. The filtering method (N = none; L = light trimming; H = heavy trimming) is given next to the source id in the upper right corner. The red vertical line indicates the frequency corresponding to the optical rotation period. The two dashed curves indicate 1% and 0.1% FAP thresholds (see text). The most likely X-ray period is reported in the upper right corner (with in parenthesis the ratio P_X/P_{opt}) along with the FAP. *Third panel*: light curve folded with the most likely X-ray period, reported in the upper right corner along with the relative modulation amplitude. Different symbols and colors indicate data points belonging to different modulation cycles. The solid gray line indicate the average count-rate as a function of phase. *Bottom panel*: light curve folded with the optically determined rotation period. [*See the electronic edition of the Supplement for Figs. 5.1–5.34*]

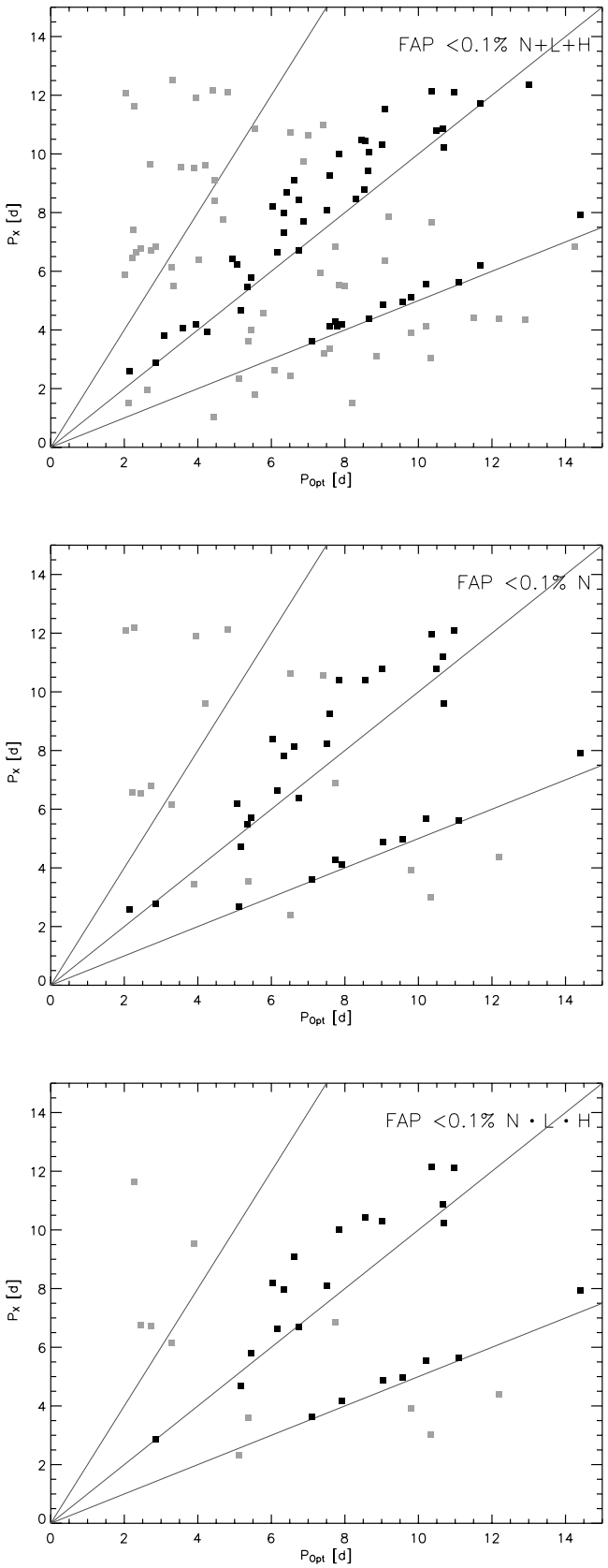

FIG. 6.—Scatter plot of the optical vs. X-ray periods. The three panels refer to three different source samples: (*top*) N+L+H with FAP $< 0.1\%$ in at least one of the filtered light curves; (*middle*) "N" with FAP $< 0.1\%$ in the nonfiltered light curve; (*bottom*) N·L·H with FAP $< 0.1\%$ in all three filters. Darker dots indicate sources with $P_X \sim P_{opt}$ or $P_X \sim \frac{1}{2}P_{opt}$, i.e., those lying in the two main peaks in the histograms in Fig. 7; lines indicate loci where $P_X = \left[\frac{1}{2},\ 1,\ 2\right]P_{opt}$.

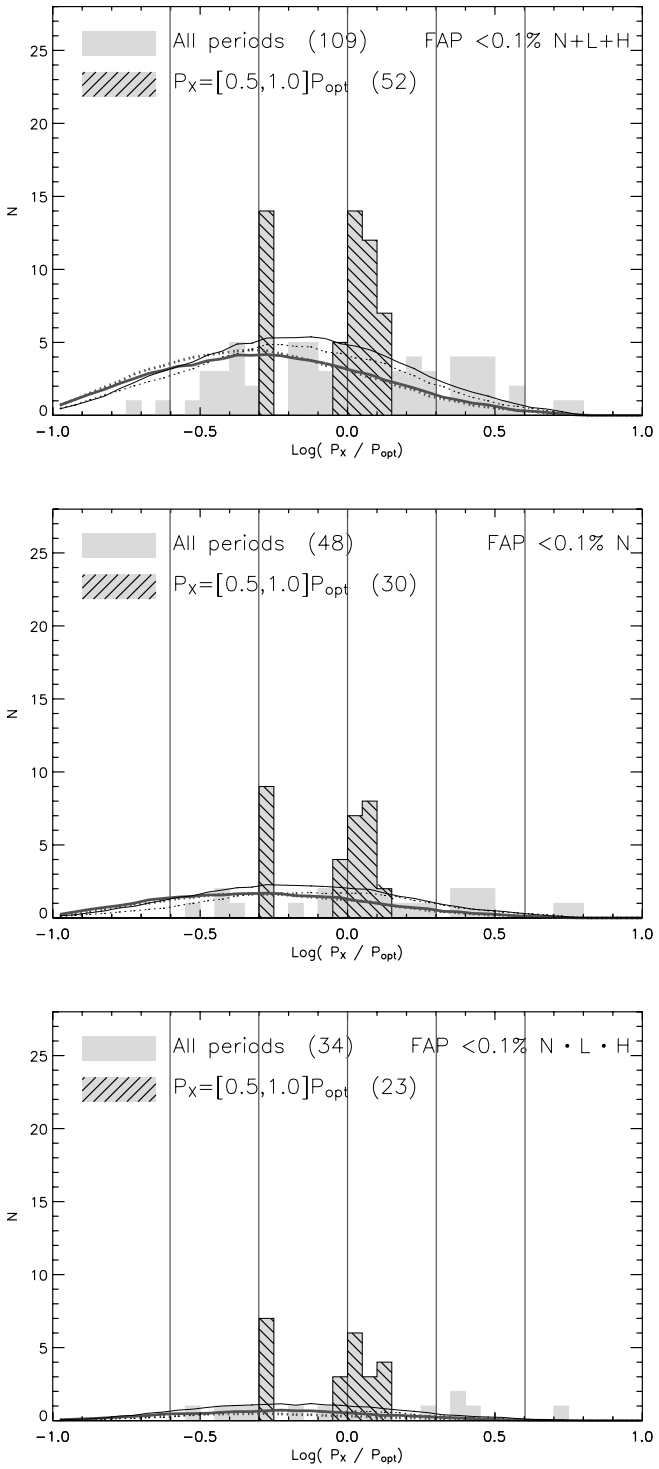

FIG. 7.—Distribution of the logarithm of the ratio between X-ray and optically determined periods for X-ray periods with FAP $< 0.1\%$ and three different choices of light curve filtering strategy as in Fig. 6. Also shown (*curves*) are distributions resulting from the simulation of unmodulated flaring light curves (see Fig. 14). Vertical lines indicate ratios of 1/4, 1/2, 1, 2, and 4.

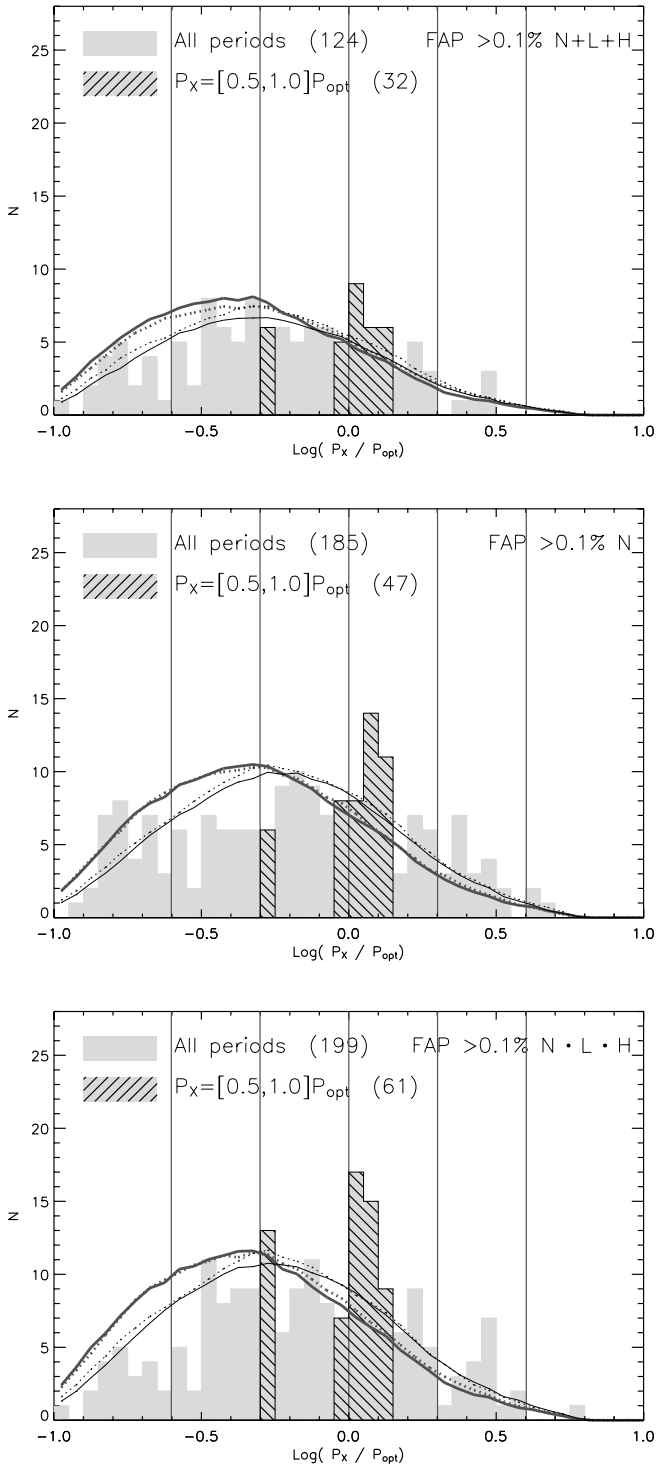

FIG. 8.—Distribution of X-ray and optical periods, as in Fig. 7, for COUP sources without significant periodic signals (FAP $> 0.1\%$). Note that the peaks present in the previous figure have here largely disappeared.

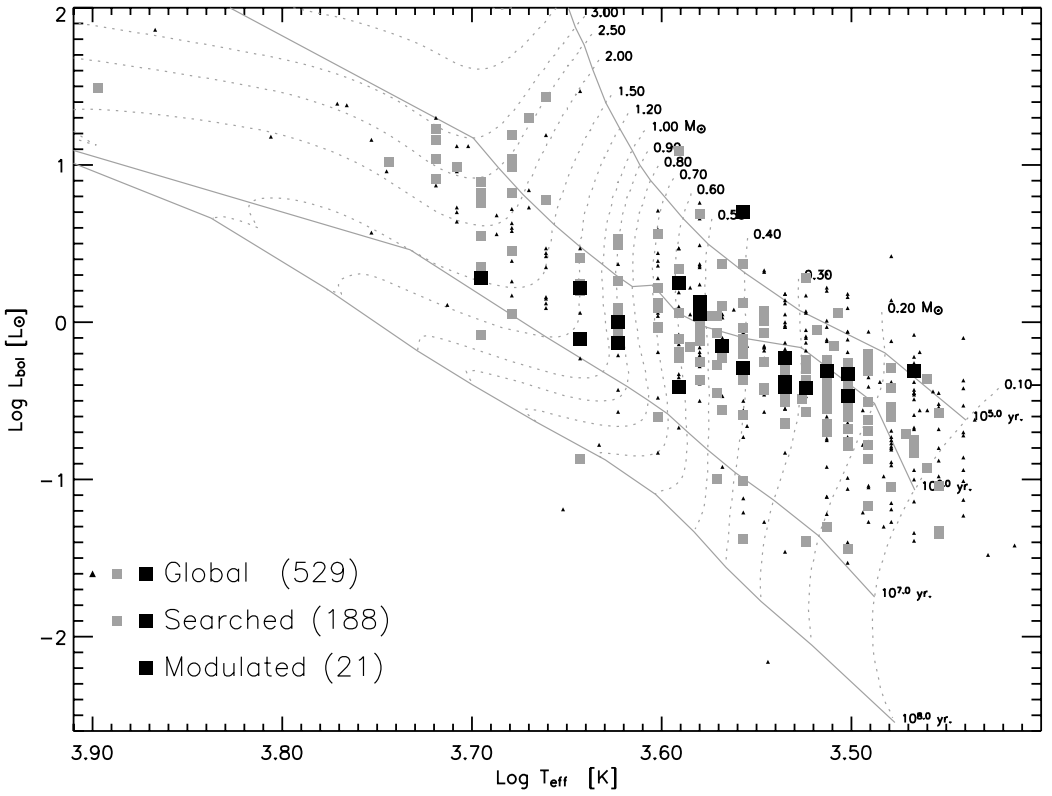

FIG. 9.—HR diagram for all COUP sources with >100 ACIS counts ("global"), for the sample for which we performed the period analysis ("searched") and for the subsample of this latter for which we found X-ray periods with FAP < 0.1% ("modulated").

related to L_X) and average optical luminosity. Within the "searched" sample there is a tendency to find more X-ray modulated stars at high L_X-values or, equivalently, high count rates. For example, within the 36 stars in the "searched" sample with 30.5 ergs s^{-1} < $\log L_X < 31$ ergs s^{-1}, about 20% (7 stars) are modulated, while the same fraction for the 45 stars with $\log L_X < 29.5$ ergs s^{-1} is only 2% (1 star). This effect is likely a bias due to photons statistics: the more photons in our light curves, the more easily we detect periodicity. The L_X/L_{bol} distributions of "searched" and "modulated" stars are instead statistically indistinguishable. Due to the bias in the "searched" sample, however, most of the "modulated" stars have high values of $L_X/L_{bol} \sim 10^{-3}$.

We investigated possible dependences of the periodicity detection fraction from an indicator of mass accretion, the equivalent width of the Ca II ($\lambda = 8542$ Å) line, and from an indicator of disk presence, the $\Delta(I - K)$ excess, both reported by Hillenbrand (1997). Any such effect would indicate a difference in the spatial distribution of X-ray–emitting plasma surrounding CTTSs and WTTSs. No striking trend in the modulation detection fraction was found. However, with both indicators, we found a hint (significance ~1%) that stars with $P_X/P_{opt} \sim \frac{1}{2}$ preferentially are accreting and have disks.

Finally, we have searched for correlations of the relative modulation amplitudes with mass, Ca II, $\Delta(I - K)$, L_X, L_X/L_{bol}, P_X, and P_X/P_{opt}, without finding any.

5. DISCUSSION: THE GEOMETRY OF PMS X-RAY–EMITTING STRUCTURES

5.1. *Summary of Main Findings and Astrophysical Background*

We have searched for rotational modulation of X-ray emission in a sample of 233 ONC stars. These are all stars with rotational period larger than 2 days known from optical photometric studies and with more than 100 counts collected in the COUP data set. This sample spans the wide mass and age range of ONC members ($0.1\ M_\odot < M < 3\ M_\odot$, 10^5 yr $< t < 10^7$ yr). We reliably detect rotational modulation with amplitudes between 20% and 70% in 23 stars or ~10% of the searched sample. For 16 sources, the X-ray emission is modulated at periods very close to the optical rotational periods, while for the remaining 7 cases the X-ray period is about one-half of the optical period. We further identify 86 stars where some evidence for modulation is found. Many, but likely not all, of these periodicities are spurious due to the difficulties in accounting for X-ray flares and other nonrotational variability. The 23 stars with rotation related modulation have higher than average X-ray luminosities with respect to stars in the searched sample, likely a bias due to the analysis. In all other respects they share the same physical properties—mass, age, and accretion—of the searched sample. Based on these results and on previous finding summarized below, in the next subsection we discuss implications for the geometry of the X-ray–emitting plasma on our young stellar systems.

The high temperatures and rapid variations of PMS X-ray emission, amply demonstrated in COUP light curves, implies that X-ray–emitting plasma must be confined by magnetic fields and heated by violent magnetic reconnection events. In isolated, older, magnetically active stars, these magnetic fields are thought to be similar to those that are observed in the solar corona, mostly small-scale loops that connect spots of different magnetic polarity on the photosphere.

But the configuration of the confining magnetic field around young PMS stars might be more complicated, as these stars are often surrounded by circumstellar accretion disks. A variety of

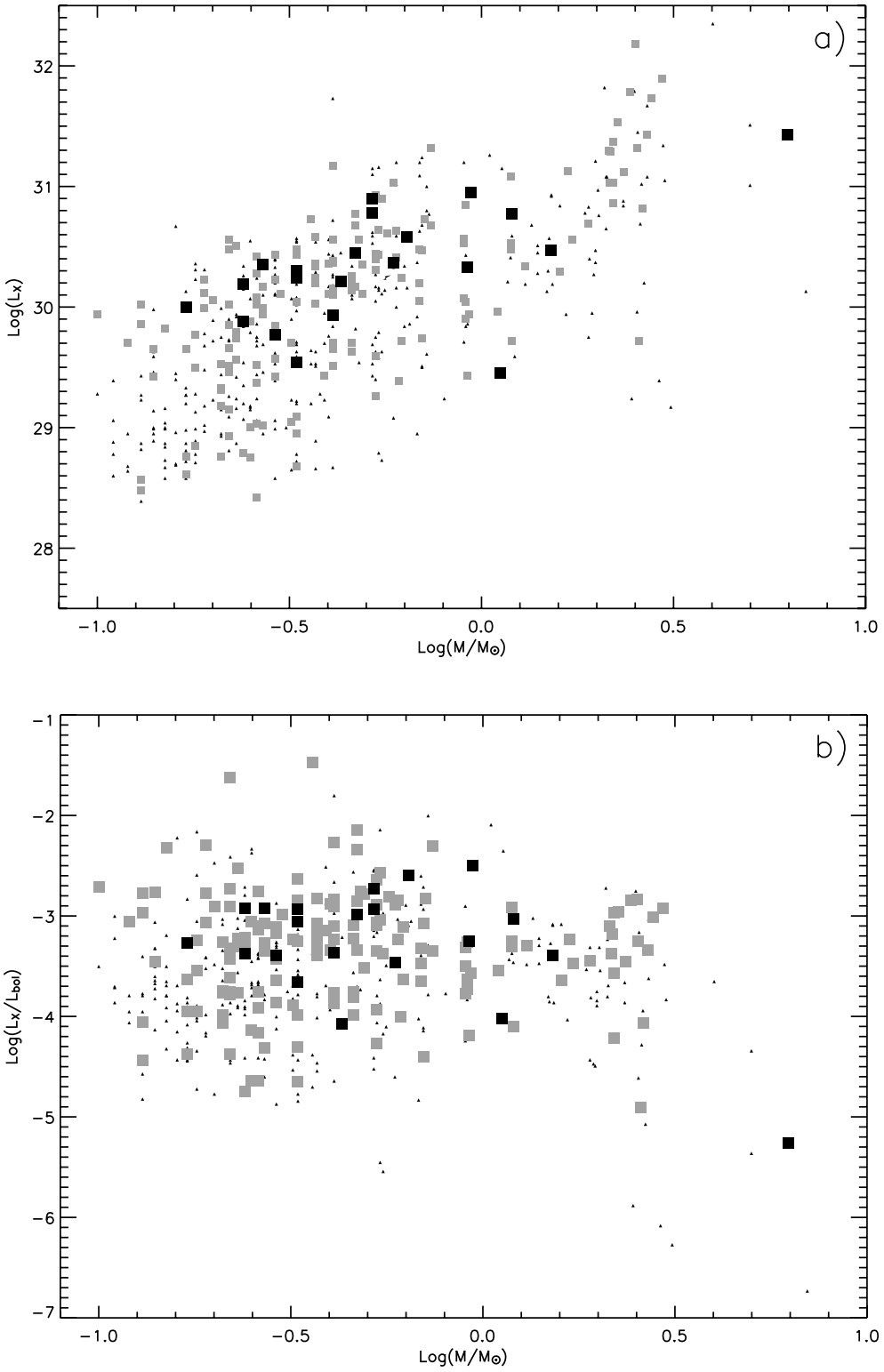

FIG. 10.—Log(mass) vs. (*a*) log (L_X) and (*b*) log (L_X/L_{bol}) for all COUP sources with mass estimates. Symbols as in Fig. 9.

astrophysical models developed with a variety of motivations suggest that the PMS stellar magnetic field extends out 5–10 stellar radii to the inner edge of the disk and interacts strongly with disk material (e.g., Königl 1991; Calvet & Hartmann 1992; Collier Cameron & Campbell 1993; Shu et al. 1994). This results in funneling some disk material in an accretion flow, launching other disk material outward into jets and outflows, and locking the stellar rotation to corotate with the inner disk. There have been suggestions that, due to shear and instabilities, magnetic reconnection will occur in these long star-disk loops, producing X-ray–emitting plasma (e.g., Hayashi et al. 1996; Shu et al. 1997; Montmerle et al. 2000; Isobe et al. 2003). However, the detailed properties of X-ray emission, together with extensive evidence for multipolar fields on PMS stellar surfaces, have generally supported a more standard stellar activity model as applied to older stars such as dMe flare and RS CVn systems

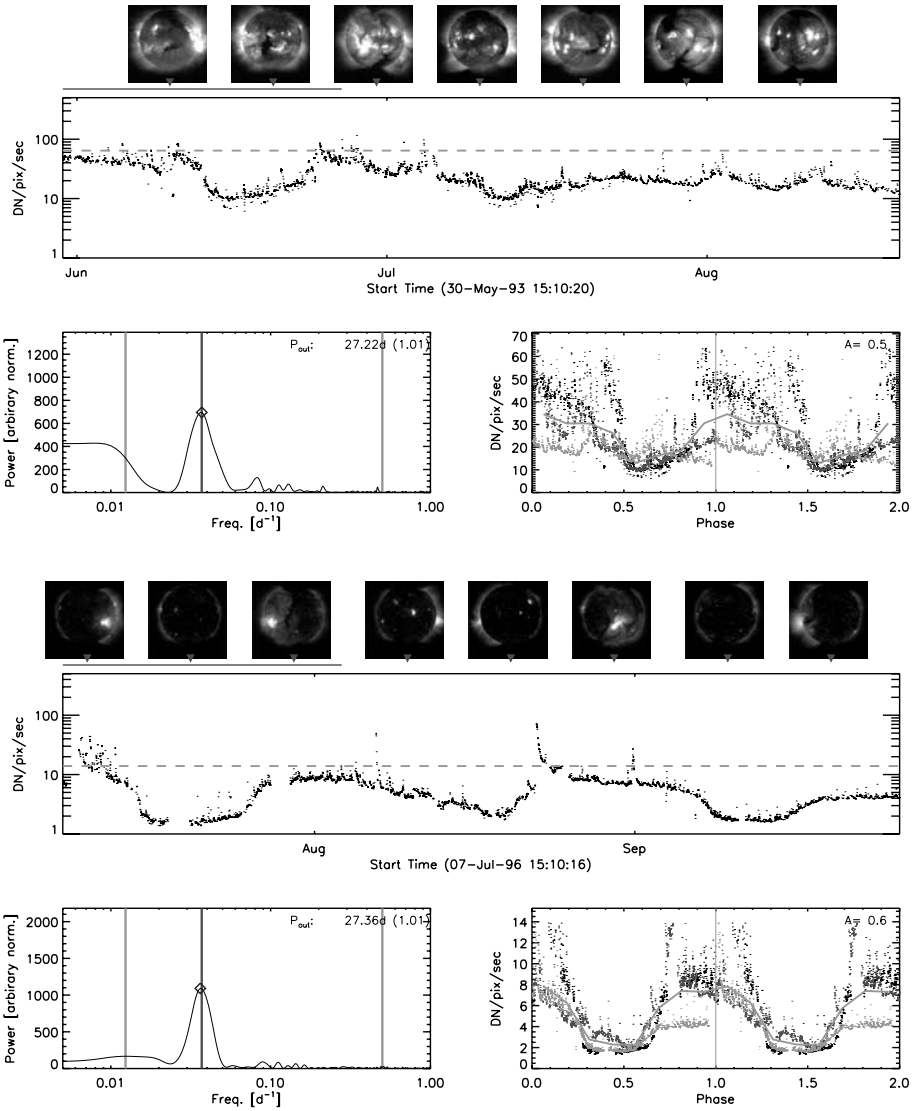

FIG. 11.—*Yohkoh* SXT (AlMg filter) light curves with relative full disk images (at selected times), periodograms, and folded light curves, in a format similar to Fig. 2. The two sets of panels refer to different 81 days time segments: the upper one is close to solar maximum, the lower one to solar minimum. [*See the electronic edition of the Supplement for a color version of this figure.*]

(see reviews by Feigelson & Montmerle 1999; Favata & Micela 2003; Güdel 2004). Perhaps the first direct indication that the observed X-rays may sometimes arise from large-scale star-disk structures arises from detailed modeling of powerful flares observed during the COUP observation (Favata et al. 2005).

5.2. *Implications of the X-Ray Rotational Modulations*

The detection of modulation of X-ray emission at periods related to the stellar rotation period in ∼10% of COUP stars has three immediate implications:

1. The X-ray–emitting structures are directly associated with the stellar surface. This precludes the rarely considered model that both footpoints of the flaring magnetic loops reside in the shearing circumstellar disk (Romanova et al. 1998).

2. The X-ray–emitting structures are not homogeneously distributed in longitude on the stellar surfaces. The amplitudes of the modulations seen in the 23 periodic COUP stars range from 20% to 70% (Table 2, col. [13]), indicating that the hemispheric brightness differences can reach roughly a factor of 2:1.

3. The bulk of the plasma emitting in the *Chandra* 0.5–8 keV band is confined in magnetic structures that, in order to undergo eclipse from the rotating star, may not extend to distances larger than $\sim R_\star$ from the stellar surface. This conclusion is not entirely inescapable if special geometries are considered. For example, eclipses could occur if the X-ray emission arises from the footpoints of corotating star-disk loops when the disk is viewed nearly edge-on. This and other similar possibilities we could think of seem unlikely to occur in 10% of otherwise ordinary PMS stars in the Orion Nebula Cluster. We thus view the detection of periodic X-ray modulations related to the optical rotation period to be a solid indication that in these stars the X-ray–emitting structures responsible for the observed modulation are compact with characteristic lengths $l \lesssim R_\star$ or $l \ll R_\star$.

It seems likely that, due to the challenges of reliably detecting periodic modulations in COUP stars, more than 10% of the stars have intrinsic X-ray periodic modulations. Three types of stars will be missed by our analysis: stars with small X-ray periodic amplitudes compared to aperiodic variations such as Poisson noise and flares; stars with large-scale inhomogeneous X-ray structures viewed too close to their rotational axis for self-eclipsing to occur; and stars with several or many small-scale

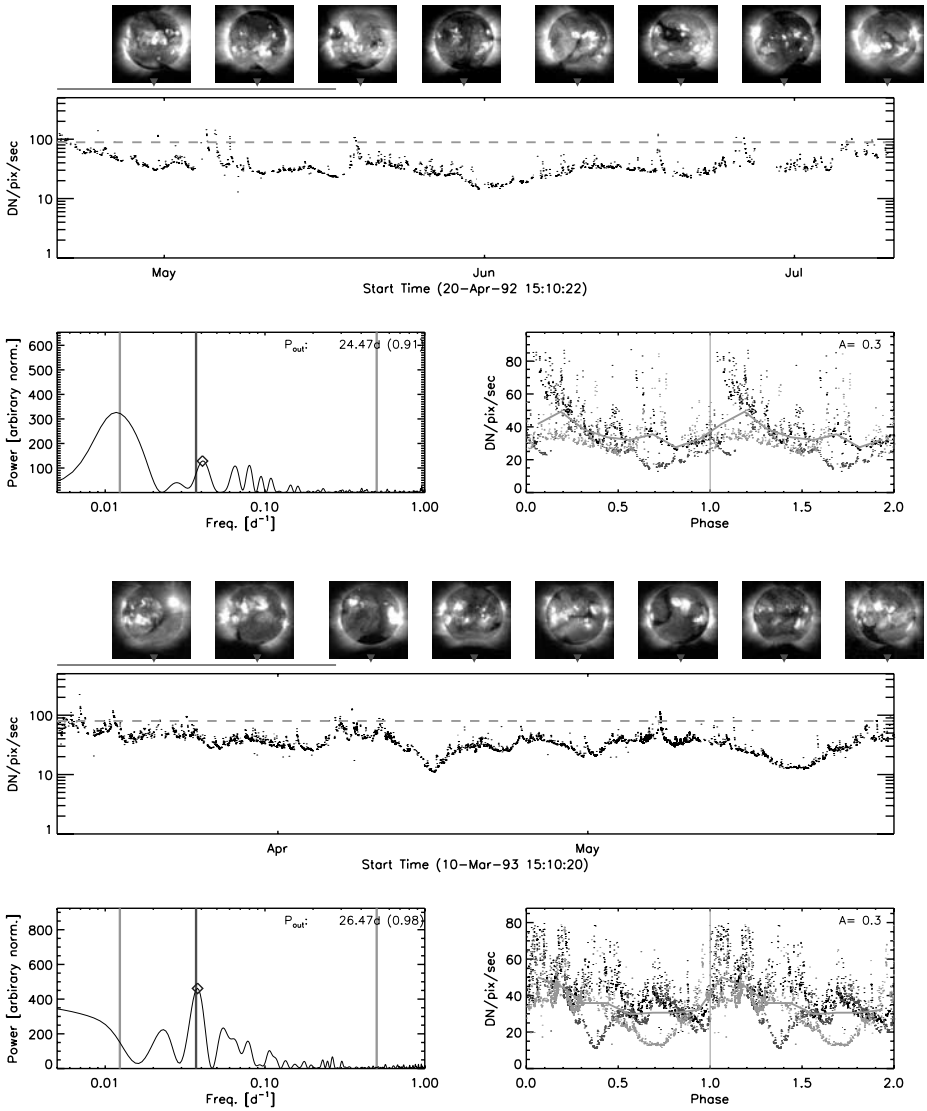

FIG. 12.—Same as Fig. 11, for two other time segments both close to solar maximum. [*See the electronic edition of the Supplement for a color version of this figure.*]

inhomogeneities. In this last case, some bright features emerge from eclipse as others enter eclipse, so the net rotational modulation has smaller amplitude than the smaller scale spatial variations. This scenario of multiple X-ray hot spots near the surface is supported by our discovery of several COUP stars with $P_X = 0.5P_{opt}$, attributable to the eclipses and emergences of bright areas on opposing hemispheres. We thus conclude that *at least* 10% of COUP stars have large-scale structure in the longitude distribution of the X-ray–emitting loops on scales less than a stellar radius.

Perhaps the most valuable inference that emerges from our findings concerns the enigma of "saturation" in magnetically active stars. Our low-mass modulated stars have very high levels of $\log L_X/L_{bol}$ (Fig. 10*b*). Excluding one high-mass star (COUP 1116, $M \sim 6\ M_\odot$) the median value is -3.05, basically the saturation level seen in magnetically active stars. At least for these stars, we can exclude one of the several suggested explanations for saturation (§ 1): it cannot arise due to a uniform filling of the stellar surface with X-ray–emitting plasma. A surface fully covered with X-ray loops would limit rotational modulation to a very low level. We note that, if we assume a solar-like picture for the X-ray–emitting regions and their relation with stellar photospheres, our finding is in agreement with the existence on these stars of photospheric inhomogeneities similar to solar spots, as inferred from optical rotational modulation.

5.3. *Comparison with the Sun*

It is helpful to consider the Sun, the only star for which we have directly imaged longitudinal X-ray structures over many years. The astronomical and astrophysical similarities between the Sun and magnetically active stars has been well documented (Schrijver & Zwaan 2000). It is important to keep in mind that the solar X-ray corona is certainly very different from that of our PMS stars. It is rotating much slower, has a much softer X-ray spectrum (even during flares) and is hugely less luminous. Latitude distributions of active regions may differ in PMS stars, and viewing orientations will be random rather than optimized for rotational eclipses.

The *Yohkoh* Soft X-ray Telescope (Tsuneta et al. 1991) has obtained an almost continuous time series of disk integrated solar fluxes comprising ~150,000 measurements in its AlMg band (~0.4–4 keV) between 1991 November 10 and 2000 December 21 (both at solar maximum) and including one solar minimum around 1996–1997. Due to the SXT operating mode, times during the most energetic flares are automatically excluded

from the time series. We have analyzed this data set in a fashion similar to that performed on the ONC stars. We first divide the data into contiguous 81 day long segments, each comprising three solar rotation periods. The LNP analysis is then applied to each segment as described in § 3 searching for periods between 2 and 81 days. Figures 11 and 12 show the typical results for four segments. As with COUP stars, the panels show the X-ray light curves, LNP periodograms, and the light curves folded with the best period. On top of the light curves we show *Yohkoh* images of the solar corona at corresponding times. In all the cases shown the periodograms and folded light curves refer to the lightly trimmed (L) light curves.

Our procedures succeed in retrieving the solar rotation period $P \simeq 27.3$ days in ∼75% of the temporal segments. This is a much higher success rate than for the ONC sample. Three factors make period finding easier for the solar case: extremely strong signals, optimal inclination of the rotation axis, and flares (those not automatically excluded from the time series) with durations much shorter than the rotation period. Modulation amplitudes computed from the folded light curves range between 20% and 60% (median ∼0.35%), similar to the rotationally modulated COUP stars. There might be a tendency to have slightly lower relative amplitudes at solar maximum rather than at minimum. The shape of the light curves vary significantly between segments depending on the configuration of active regions; broadly speaking, they are similar to the ones we observed in our PMS stellar sample.

From this first comparison between stellar COUP data and the solar *Yohkoh* data we conclude that, although in PMS stars plasma emission measures and temperatures are tremendously higher, the degree of longitudinal inhomogeneity in the X-ray–emitting regions are qualitatively similar. It is thus reasonable to view both the two-dimensional surface distribution—dominated by one or a few active regions—and the three-dimensional distribution—dominated by emission close to the stellar surface—of X-ray emission in the Sun to be similar to that in PMS stars.

6. SUMMARY

We have searched for rotational modulation of X-ray emission in a sample of 233 young PMS stars in the Orion Nebula Cluster. The study was made possible by the *Chandra* Orion Ultradeep Project, which obtained an 850 ks long ACIS observation of the region during a time span of 13.2 days. In order to check that the observed X-ray modulation is related to stellar rotation, this work focused on a selected sample of stars with know rotation period.

Periodicity in binned light curves was searched with the Lomb Normalized Periodogram method. The analysis was performed both on unfiltered light curves and on light curves that were first trimmed to remove large flares. False alarm probabilities were estimated so as to take into account the presence of nonrotational short-term (<8 hr) variability such as flares; because of nonrotational variability with longer timescales, these FAPs remain indicative. We thus verified our analysis technique using extensive numerical simulations.

We reliably establish the presence of X-ray rotational modulation in 23 stars, 10% of the searched sample and the largest sample of stars of any class in which X-ray rotational modulation has been observed to date. For 86 additional stars in the searched sample the detection of rotational modulation is less reliable. Within the 23 reliable detections relative amplitudes range from 20% to 70% and periods between 2 and 12 days. In 16 cases the X-ray modulation period is similar to the stellar rotation period, while in seven cases it is about half that value. The data suggest that X-ray periods are on average 5%–10% longer than either $P_{\rm opt}$ or $0.5P_{\rm opt}$.

Comparing the stellar properties of the modulated sample to those of the searched sample, we find that the two samples are indistinguishable with respect to mass, age, and accretion disk properties. X-ray modulation is, however, detected preferentially in bright X-ray sources. We understand this as a selection effect. The data also suggest, albeit with low significance, that stars with $P_{\rm X} \sim 0.5P_{\rm opt}$ are preferentially active accretors, according to the Ca II line EW, and posses disks, according to the *K*-band excess.

Our main conclusions, referred to the stars that show modulation, are as follows:

1. X-ray–emitting plasma is inhomogeneously distributed in longitude. A comparison with solar data suggests a similar degree of inhomogeneity.
2. Saturation of activity, $L_{\rm X}/L_{\rm bol} \sim 10^{-3}$, is not due to the filling of the stellar surface with active region.
3. Dominant emitting structures are likely compact with sizes $\lesssim R_\star$.

The last conclusion may seem in contrast with that of Favata et al. (2005) based on the analysis of the decay phase of the most luminous flares observed during the COUP observation. Favata et al. (2005) find that a number of large flares can be modelled only by assuming very long magnetic loops ($5–20R_\star$). It is not yet clear how common these large loops structures are. It is conceivable that long-lived compact structures are the most common and that they coexist with extended ones that may become prominent during flares.

The authors are grateful to K. Stassun, S. Shang and S. Orlando for useful discussion. COUP is supported by *Chandra* Guest Observer grant SAO GO3-4009A (PI: E. Feigelson). E. F., G. M., and S. S. acknowledge financial support from the Ministero dell'Istruzione dell'Universitá e della Ricerca. E. D. F. is also supported by ACIS Team contract NAS8-38252.

Facilities: CXO (ACIS-I)

APPENDIX

SIMULATIONS OF COUP X-RAY LIGHT CURVES

This Appendix describes the development of simulated X-ray light curves to test the performance of our analysis techniques in data sets suffering the realistic complexities seen in COUP ONC X-ray light curves. These include repeated high-amplitude flaring, longer-timescale aperiodic variations, gaps in the exposure due to the *Chandra* orbital perigees, and Poissonian noise. Other currently unknown sources of variability might also be present. We focus much attention on the effect of flares on the period detection procedures. Simulating realistic light curves is not straightforward because it requires the knowledge of several input quantities that are at present not well constrained, such as the flare frequency, distributions of flare amplitudes and durations, and the relative

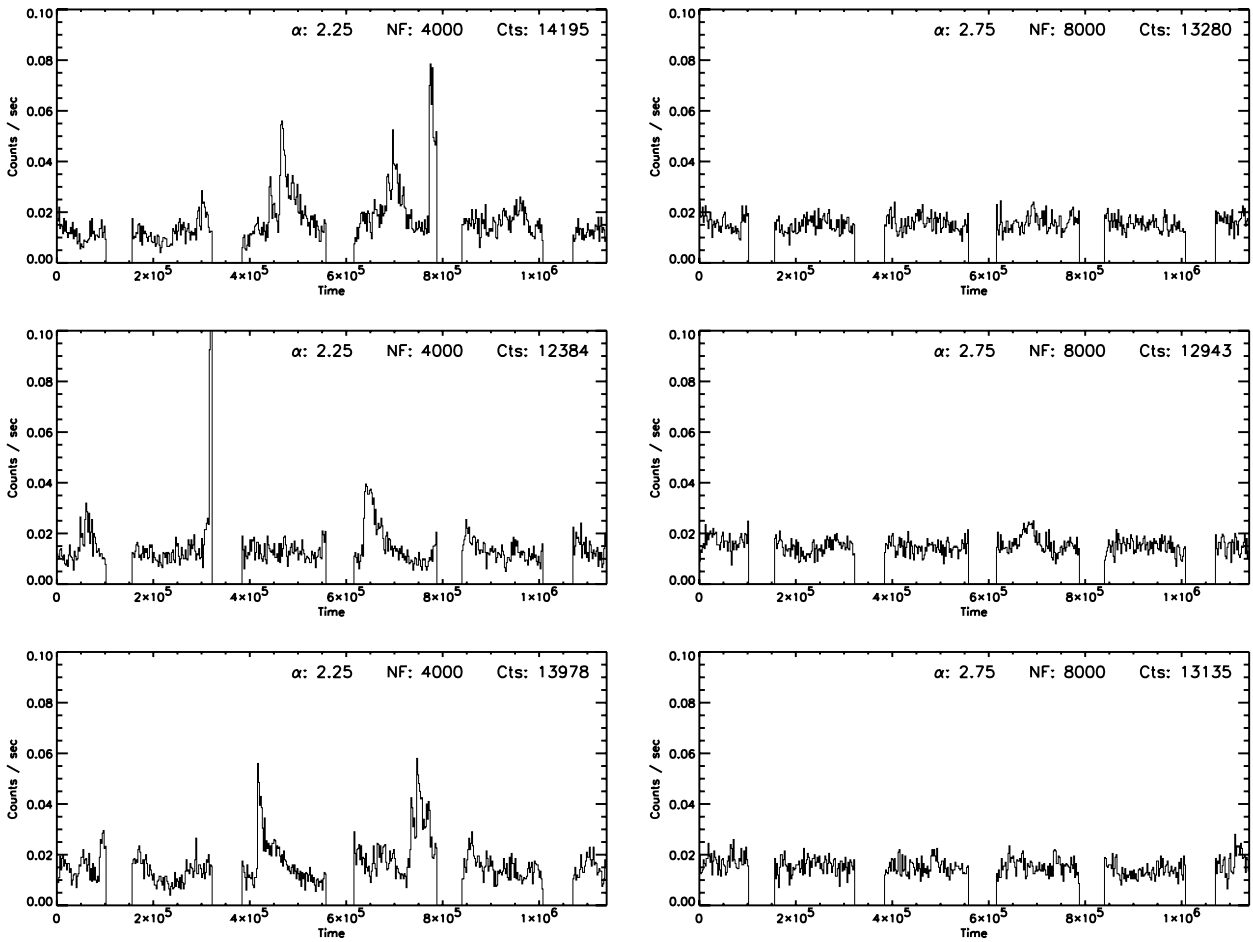

FIG. 13.—Example of six simulated light curves with no modulation, three for each of two values of the parameter α (=the slope of the flare intensity distribution): $\alpha = 2.25$ (*left*) and 2.75 (*right*). The number of simulated flares (NF), all having $\tau_{\rm fl} = 5$ hr, is chosen so to yield, in the two cases, a similar average number of counts. The actual number of simulated counts is given in the upper right corner of each panel.

contribution of flares and "quiescent" emission, if at all present. These issues are studied for a small sample of 1 $M_\odot$ COUP stars by Wolk et al. (2005) but have not yet been characterized for the full COUP sample.

We therefore introduce a model of the stellar X-ray emission that is simple enough to be described with few parameters, but still yields light curves that qualitatively resemble observed ones. The model light curves are made exclusively out of a distribution of flares based on the well-studied idea that even stellar "quiescent" emission arises from the superposition of many microflares (Kashyap et al. 2002 and references therein). Forthcoming COUP studies will tackle this issue in greater detail. Here we introduce this model exclusively as a tool to produce useful light curves.

A1. CONSTRUCTION OF SIMULATED LIGHT CURVES

The following procedure was followed for creating unmodulated light curves:[15]

1. Generate a specified number, NF, of random flare start times, uniformly distributed between $t_0 - 3\tau_f$ and t_1, where t_0 and t_1 are the start and end times of our COUP observation and $\tau_{\rm fl}$ is a specified decay timescale for flares.
2. Assign to each of the NF flares an intrinsic amplitude, C_0 or total number of counts, obtained from the probability distribution $dn/dC_0 \propto C_0^{-\alpha}$, where α is a specified power-law index of the flare intensity distribution. We find (see below) that the observed data are best reproduced by α larger than two. To avoid an energy divergence of small flares, we arbitrarily adopt a lower limit $C_0 > C_{\rm min} = 1$ of flare intensities.[16]
3. Compute the observed amplitude C for each flare, randomly taken from a Poisson distribution with mean C_0.
4. Simulate C photons arrival times for each flare, assuming an instantaneous rise and an exponential decay with a decay time $\tau_{\rm fl}$.
5. Merge the arrival times for each flare so to generate the simulated light curve.
6. Filter out simulated events that fall outside the Good Time Intervals of the COUP observation (i.e., in the gaps due to the *Chandra* satellite orbital perigee).

[15] Throughout these simulations we will neglect background contributions to the light curves. This is justified by the relative uninportance of background for the majority of COUP sources (Getman et al. 2005), implying that the noise properties of real background-subtracted light curves are very similar to those of background-free simulated light curves.

[16] Corresponding to a minimum flare energy $\sim 5 \times 10^{32}$ ergs.

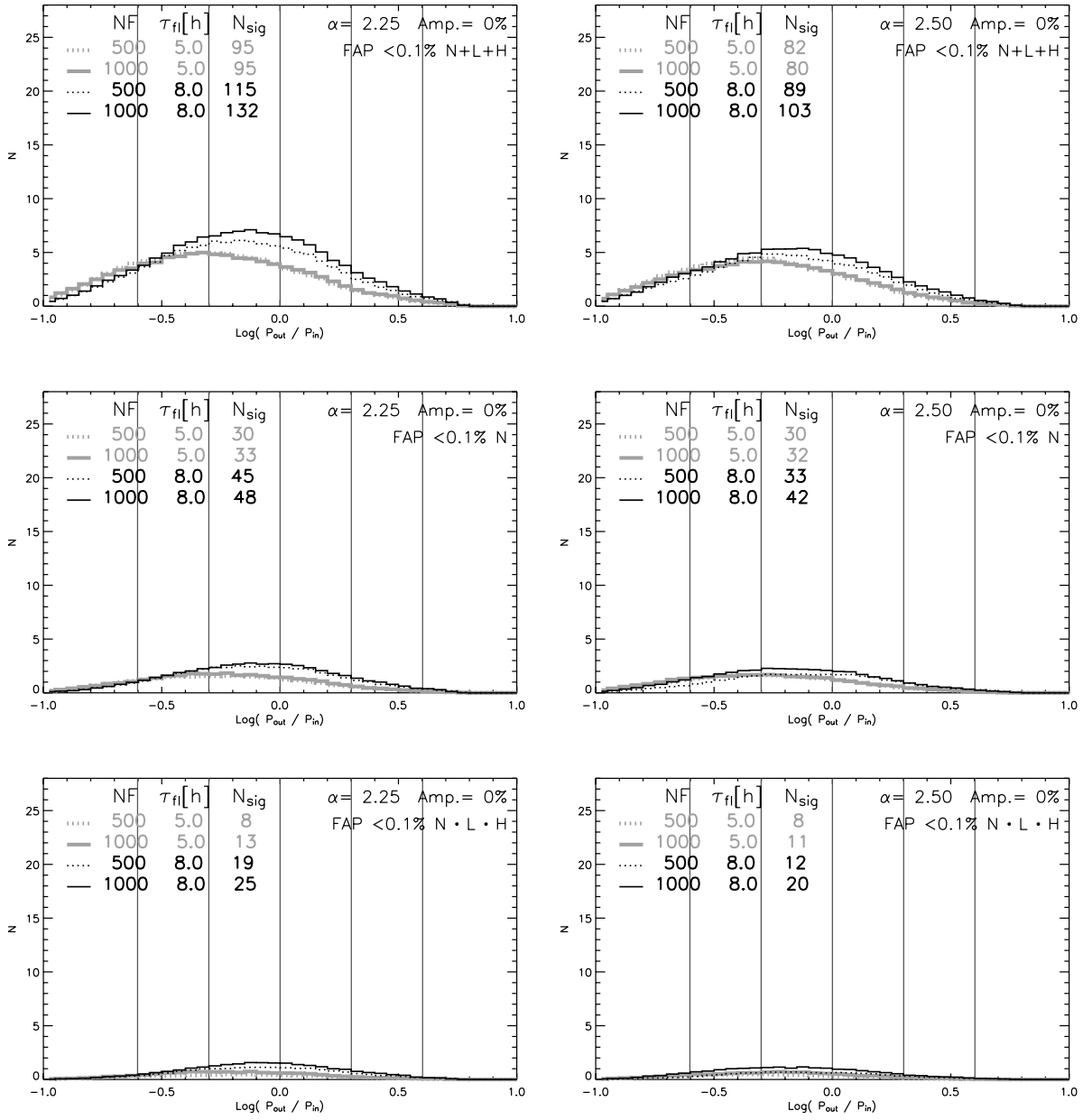

FIG. 14.—Histograms of $\log P_{\rm out}/P_{\rm in}$, resulting from the application of our period finding method to simulated "flaring" light curves (see text) with no intrinsic modulation (Amp. = 0%). Rows refer to three selections of "significant" periods, the same as in Fig. 7. *From top to bottom*: N+L+H, N, and N·L·H. The left and right columns refer to simulations with $\alpha = 2.25$ and $\alpha = 2.50$. Within each panel four histograms are shown, for NF = 500 and 1000 and for $\tau_{\rm fl} = 5$ and 8 hr, as indicated in the legend on the upper left of each panel. All histogram are normalized so to yield the expected distributions for a sample of 233 stars with $P_{\rm in}$ equal to $P_{\rm opt}$ in our "searched" sample. In the legend we also report the integral of these distributions, $N_{\rm sig}$, indicating for each set of input parameters the total number of stars expected to pass the significance selections.

Having fixed $C_{\rm min}$, the free parameters in the model are α, the steepness of the flare amplitude distribution, NF, the number of flares, and $\tau_{\rm fl}$, the flare decay time. We consider two values of $\tau_{\rm fl}$, 5 and 8 hr, consistent with the typical flare durations seen in COUP light curves. Setting NF is equivalent to setting the total counts for the source. We examined light curves produced with values of α ranging between 2.0 and 3.0. The flatter $\alpha = 2.0$ distribution produces light curves with far too many bright flares compared to typical COUP light curves, while $\alpha = 3.0$ clearly results in too few bright flares. Figure 13 shows six examples of simulated light curves.

In order to simulate rotational modulation, we modify the distribution from which flare start times are drawn (step 1) from a constant distribution to a sinusoidal one with a given input period ($P_{\rm in}$) and amplitude (Amp.). We then apply our period searching methodology (§ 3) to all simulated light curves, including attempts to trim flares, calculation of LNPs, estimation of FAPs, and selection of significant results according to various criteria.

We initially ran these simulations choosing the input parameters from the following grid: $\alpha = 2.0$–3.0 in 0.25 steps, NF = 500, 1000, and 2000, Amp. = 0%–100% in 20% steps. Values of $P_{\rm in}$ were chosen equal to the optically determined rotation periods of the 233 stars in our main sample, repeated five times so as to have, for each choice of the other parameters, 1165 simulated light curves with $P_{\rm in}$ distributed as $P_{\rm rot}$. The value of α was constrained using two simple strategies to compare real and simulated light curves with a similar number of counts: visual examination of simulated and real light curves, and comparison of the standard deviation of the

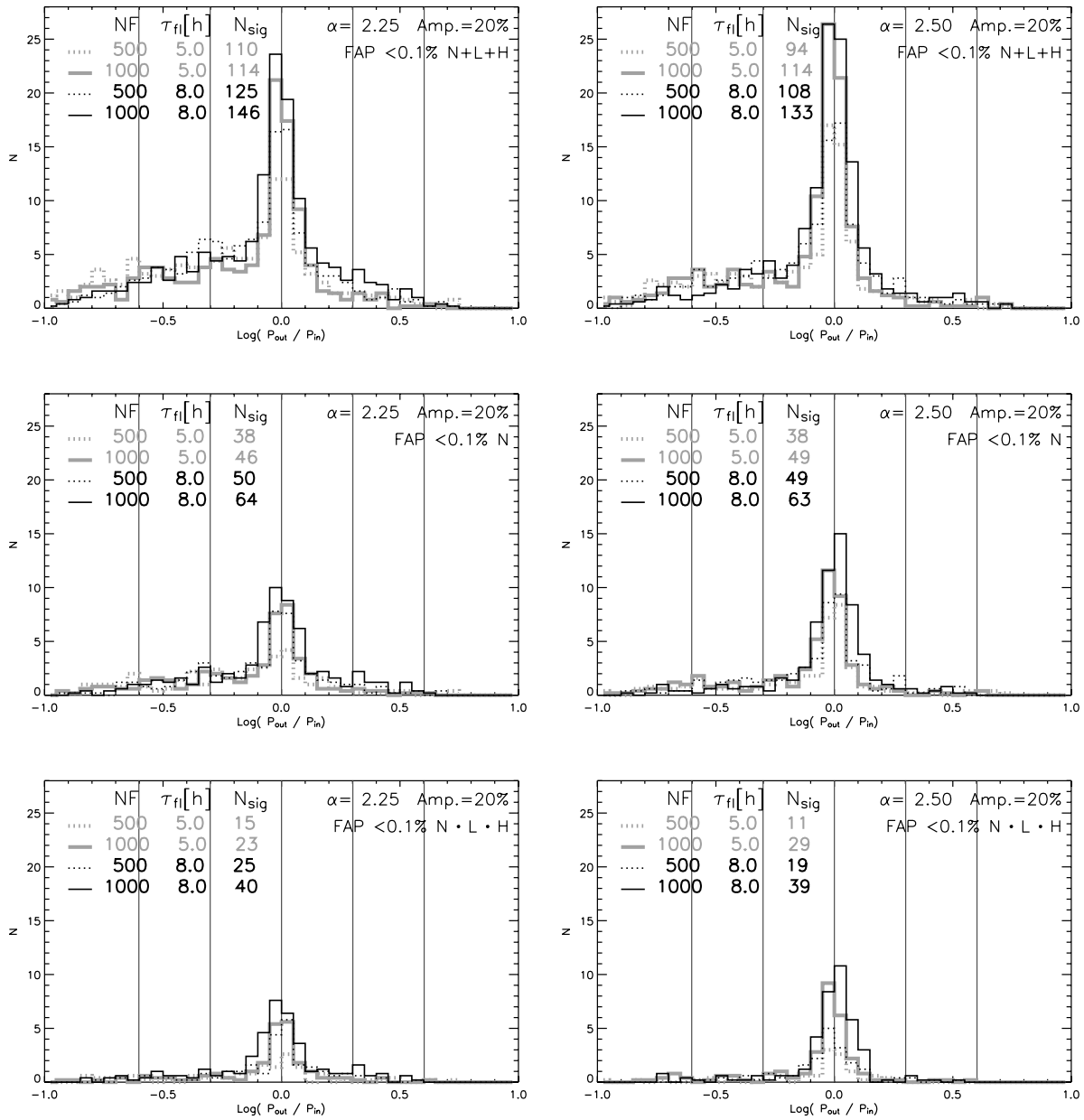

FIG. 15.—Same as Fig. 14, but for simulated light curves with intrinsic 20% relative modulation.

count rates in the binned light curves. Both of these qualitative comparisons indicate that α between 2.25 and 2.5 gives light curves that most resemble the observed ones. With these choices of α, the NF (number of flares) that reproduces the median observed number of counts in our "searched" sample ($\sim$2300) is between 500 and 1000. Simulations using these parameters, with and without periodic modulations applied, were then used to study the performance of our period finding method.

A2. RESULTS FOR SIMULATED UNMODULATED COUP SOURCES

Simulations with Amp. = 0.0 are valuable to testing the false alarm probabilities that may lead to spurious period detections. Figure 14 shows, in the same format of Figure 7 with actual COUP data, the distributions of $\log P_{\rm out}/P_{\rm in}$, for the three selections of "significant" periods (N+L+H, N, and N·L·H) and for our chosen ranges of model input parameters. The histograms are normalized to yield the expected distributions for our "searched" sample. Since the simulated light curves are not modulated, there is no relation between input and output period. The shape of the simulated distributions therefore solely reflects the distribution of *spurious* detected X-ray periods with respect to the input optical stellar rotation periods. The distributions show that using a realistic model of the X-ray emission from ONC stars:

1. Detection of spurious periods due to our failure to properly account and/or remove flares cannot explain the observed sharp peaks in the observed $P_{\rm X}/P_{\rm opt}$ histogram.
2. Flares can account for most or all of the X-ray periods that do not fall within these peaks and that are therefore unrelated to optical periods. It is also apparent that the number of spurious periods found in these unmodulated light curves is largest when

accepting periods that have FAP $< 0.1\%$ in any of the three analyzed light curves (the "N+L+H" sample) and lowest when accepting only periods with FAP $< 0.1\%$ in all three analyses (the "N·L·H" sample).

A3. RESULTS FOR SIMULATED MODULATED COUP SOURCES

Figure 15 shows in the same format results for simulated light curves with a small, 20%, intrinsic modulation. Success in retrieving the input periods would be indicated by a narrow peak at $\log P_{\rm out}/P_{\rm in} = 0$ containing the largest possible fraction of the 233 input sources. We find that most periods can be retrieved using our method, most cleanly in the N·L·H selection that includes heavy trimming of flares. Tails of spurious periods are found. Note that it is easier to retrieve the input periods for the larger value of α (i.e., when large flares are less frequent) and for the larger number of flares, NF (i.e., when the total source counts are higher). Larger relative modulation amplitudes (not shown) also result in higher success rates. Several other indications can be read from Figure 15 as well as from similar ones for the other amplitudes:

1. The uncertainties in the derived period, i.e., the width of the peak in the $P_{\rm out}/P_{\rm in}$ ratio histograms are of the same order of the width in the corresponding plot based on real COUP data.
2. Aliases of the input periods are *not* seen in the simulations, such as the $P_{\rm X} = 0.5P_{\rm opt}$ secondary peak clearly seen in the real COUP data. We only obtain a peak at $P_{\rm out}/P_{\rm in} = 1$ and a scattered tail in the range $0.2 < P_{\rm X}/P_{\rm opt} < 5$.
3. No systematic shift between $P_{\rm out}$ and $P_{\rm in}$ is observed.
4. Short periods are determined more precisely (not shown). This occurs because more modulation periods are covered by the observation. It might also explain the smaller width of the $P_{\rm X}/P_{\rm opt} \sim 0.5$ peak in Figure 7.
5. Periods from $\sim$1 day and $\sim$13 days can be retrieved, confirming the results of the purely periodic simulations (§ 3).

REFERENCES

Calvet, N., & Hartmann, L. 1992, ApJ, 386, 239
Carpenter, J. M., Hillenbrand, L. A., & Skrutskie, M. F. 2001, AJ, 121, 3160
Collier Cameron, A., & Campbell, C. G. 1993, A&A, 274, 309
Damiani, F., & Micela, G. 1995, ApJ, 446, 341
Drake, J. J., Peres, G., Orlando, S., Laming, J. M., & Maggio, A. 2000, ApJ, 545, 1074
Favata, F., & Micela, G. 2003, Space Sci. Rev., 108, 577
Favata, F., & Schmitt, J. H. M. M. 1999, A&A, 350, 900
Favata, F., et al. 2005, ApJS, 160, 469
Feigelson, E. D., & Montmerle, T. 1999, ARA&A, 37, 363
Flaccomio, E., Micela, G., & Sciortino, S. 2003a, A&A, 397, 611
Flaccomio, E., et al. 2003b, ApJ, 582, 398
Getman, K. V., et al. 2005, ApJS, 160, 319
Grosso, N., et al. 2005, ApJS, 160, 530
Guedel, M., Schmitt, J. H. M. M., Benz, A. O., & Elias, N. M. 1995, A&A, 301, 201
Güdel, M. 2004, Astron. Astrophys. Rev., 12, 71
Hayashi, M. R., Shibata, K., & Matsumoto, R. 1996, ApJ, 468, L37
Herbst, W., Bailer-Jones, C. A. L., Mundt, R., Meisenheimer, K., & Wackermann, R. 2002, A&A, 396, 513
Herbst, W., Rhode, K. L., Hillenbrand, L. A., & Curran, G. 2000, AJ, 119, 261
Hillenbrand, L. A. 1997, AJ, 113, 1733
Hussain, G. A. J., et al. 2005, ApJ, 621, 999
Isobe, H., Shibata, K., Yokoyama, T., & Imanishi, K. 2003, PASJ, 55, 967
Jardine, M., Wood, K., Collier Cameron, A., Donati, J.-F., & Mackay, D. H. 2002, MNRAS, 336, 1364
Jones, B. F., & Walker, M. F. 1988, AJ, 95, 1755
Kashyap, V. L., Drake, J. J., Güdel, M., & Audard, M. 2002, ApJ, 580, 1118
Kastner, J. H., Huenemoerder, D. P., Schulz, N. S., Canizares, C. R., & Weintraub, D. A. 2002, ApJ, 567, 434
Königl, A. 1991, ApJ, 370, L39
Lafler, J., & Kinman, T. D. 1965, ApJS, 11, 216
Lucas, P. W., & Roche, P. F. 2000, MNRAS, 314, 858
Marino, A., Micela, G., Peres, G., & Sciortino, S. 2003, A&A, 407, L63
Montmerle, T., Grosso, N., Tsuboi, Y., & Koyama, K. 2000, ApJ, 532, 1097
Muzerolle, J., Calvet, N., & Hartmann, L. 2001, ApJ, 550, 944
Orlando, S., Peres, G., & Reale, F. 2001, ApJ, 560, 499
Pizzolato, N., Maggio, A., Micela, G., Sciortino, S., & Ventura, P. 2003, A&A, 397, 147
Preibisch, T., et al. 2005, ApJS, 160, 401
Romanova, M. M., Ustyugova, G. V., Koldoba, A. V., Chechetkin, V. M., & Lovelace, R. V. E. 1998, ApJ, 500, 703
Scargle, J. D. 1982, ApJ, 263, 835
Schmitt, J. H. M. M., Robrade, J., Ness, J.-U., Favata, F., & Stelzer, B. 2005, A&A, 432, L35
Schrijver, C. J., & Zwaan, C. 2000, Solar and Stellar Magnetic Activity (Cambridge: Cambridge Univ. Press)
Schuster, A. 1898, Terr. Mag., 3, 13
Shu, F., Najita, J., Ostriker, E., Wilkin, F., Ruden, S., & Lizano, S. 1994, ApJ, 429, 781
Shu, F. H., Shang, H., Glassgold, A. E., & Lee, T. 1997, Science, 277, 1475
Stassun, K. G., Ardila, D. R., Barsony, M., Basri, G., & Mathieu, R. D. 2004, AJ, 127, 3537
Stassun, K. G., Mathieu, R. D., Mazeh, T., & Vrba, F. J. 1999, AJ, 117, 2941
Stelzer, B., & Schmitt, J. H. M. M. 2004, A&A, 418, 687
Stelzer, B., et al. 2005, ApJS, 160, 557
Tsuneta, S., et al. 1991, Sol. Phys., 136, 37
Wolk, S., et al. 2005, ApJS, 160, 423